SLAC–PUB–5607
July 1991
(A)

THE STANFORD LINEAR COLLIDER*

J. T. SEEMAN

Stanford Linear Accelerator Center
Stanford University, Stanford, California 94309

Contributed to the Physics of Particle Accelerators

* Work supported by the Department of Energy, contract DE–AC03–76SF00515.

THE STANFORD LINEAR COLLIDER*

John T. Seeman

Stanford Linear Accelerator Center
Stanford, California, 94309

Contents:

* Work supported by US Department of Energy contract AC03-76SF-00515.

Contributed to "The Physics of Particle Accelerators", M. Month ed., AIP (1991).

THE STANFORD LINEAR COLLIDER*

John T. Seeman

Stanford Linear Accelerator Center
Stanford, California, 94309

1. INTRODUCTION

In the early 1980s the world community of high energy physics faced the challenge of building an electron accelerator to provide direct observations and detailed studies of the leptonic and hadronic decays of the then hypothesized Z^0 boson. If the Z^0 boson existed, annihilations of electrons with their antiparticles (positrons) at center of mass energies of over 90 GeV/c^2 should produce the highly sought after Z^0 decays in large quantities and with very low detector backgrounds. From this challenge emerged two electron-positron colliding beam accelerators.

The first accelerator, called the Stanford Linear Collider (SLC), was started at the Stanford Linear Accelerator Center (SLAC) in California (1-7). This linear collider could be built relatively inexpensively by using as a basis the existing two mile accelerating structure at SLAC, albeit with many modifications and additions from beginning to end. Because of the existing facilities at SLAC, this first-of-its-kind collider had the potential of producing hadronic data at the Z^0 mass before any other collider and, more importantly, of becoming a prototype of larger and more energetic linear colliders of the future (8-12). Furthermore, it was expected that during the design and commissioning of the SLC numerous advances in accelerator physics and beam diagnostics of high energy, high brightness beams would be made (13-15). These advances would have applications not only for the next generation of linear collider but also for synchrotron radiation sources, free electron lasers, high brightness beam sources, and ultra-low emittance storage rings. As with any new frontier accelerator the risks were high but so to were the rewards.

The second accelerator, called the large electron-positron project (LEP) (16,17), was started in Geneva, Switzerland, at the CERN laboratory. This large circular collider was a new facility. CERN, however, had the advantage of a twenty year history of storage ring technology and thus was expected to commission LEP rapidly. It is widely accepted that the cost of this style of collider increases approximately quadratically with beam energy (18), while the cost of a linear collider is expected to grow linearly with beam energy. Thus, the fiscal possibility of building a future electron-positron circular collider larger than LEP is remote at best.

A decade later, in the summer of 1989, the SLC was completed; it produced refined measurements of the mass (91.14 [+/- 0.12] GeV/c^2) and width (2.42 [+0.45, -0.35] GeV/c^2) of the Z^0 boson and determined the number of neutrino families (three) (19,20). Later that year LEP completed an initial data run and provided greatly improved statistical errors on the above results. Today LEP continues to produce numerous Z^0 decays each day, checking the foundations of the standard model. The SLC has turned its efforts to studying Z^0 decays with polarized electrons and studying the requirements for the next linear collider. There are few, if any, studies at the moment anywhere in the world investigating electron-positron circular colliders more energetic than LEP; whereas, many institutions around the globe are designing, constructing, and testing new devices and techniques for future high energy, electron-positron linear colliders (21).

This report discusses the new accelerator physics concepts developed and tested while making the SLC a working research tool. At present, there are more interesting accelerator physics tests being proposed each day than there is accelerator time to perform them. This pace is expected to continue into the mid-1990s. Some of the issues being explored include very small emittance bunches, beams of extremely high power densities, multiple bunch beams, beam-beam interaction, positron target design, electron gun design, low emittance damping rings, wakefield compensation, chromatic correction, halo collimation, reliability, instrumentation, and controls. In this report implications for future accelerators are indicated throughout the discussions.

This summary of SLC accelerator advances cannot possibly cover in detail the thousands of design documents, SLC Collider Notes, logbooks of observations, publications of accelerator physics and technology, and individual reports of investigations generated throughout the history of the SLC. The references contained in the bibliography are a good source for further study.

2. DESIGN CRITERIA FOR THE SLC

The SLC was designed to collide single bunches of electrons (e^-) and positrons (e^+) head-on at a single interaction point (IP) with single beam energies, E, up to 70 GeV. The design concept for the SLC was prefaced by exploratory scenarios for lepton colliders using beams from two linear accelerators (22-24). Rather than construct a second linear accelerator (linac) at SLAC to aim at the existing linac, a decision was made to accelerate both bunches in the same linac and collide them after they pass through oppositely curving arcs. The SLC collider is the highest energy accelerator that can use the arc system because synchrotron radiation losses for each particle, which grow rapidly with energy (E^4 / ρ), soon become unmanageable.

The usefulness of a collider is gauged by the time integrated luminosity with conditions acceptable for the physics detector at the IP. The luminosity L of the SLC determines the event rate R where R is the product of L and the physics cross section. The luminosity can be calculated from the parameters of the beams.

$$L = N^+ N^- f / (4 \pi \ \sigma_x \ \sigma_y) \qquad 1$$

where N^+ is the average number of positrons per bunch, N^- the corresponding number of electrons, f the collision rate, and σ_x and σ_y are horizontal and vertical bunch sizes at the IP. The bunch size is determined by the emittance ε of the beam and the betatron function β. $\sigma = [\varepsilon \beta]^{1/2}$ (25). The emittances throughout the SLC are usually stated in energy invariant units given by $\gamma \varepsilon$, where γ is the relativistic energy factor $E / m c^2$.

The highest luminosity is obtained when the bunch charges are the highest, the repetition rate is as large as possible, and the transverse bunch sizes are as small as possible. Furthermore, the physics detector at the IP desires a minimum amount of debris or backgrounds from the beam so as not to cloud or prevent data collection. However, each of these goals push the technological limits and are often strongly interrelated.

The normal collision cycle for the SLC is illustrated with Figure 1. A positron bunch and two electron bunches are extracted from their respective damping rings. The positron bunch and the first electron bunch are accelerated to 47 GeV/c^2 in the SLAC linac with a gradient of about 18 MeV/m. After they pass through the two arcs

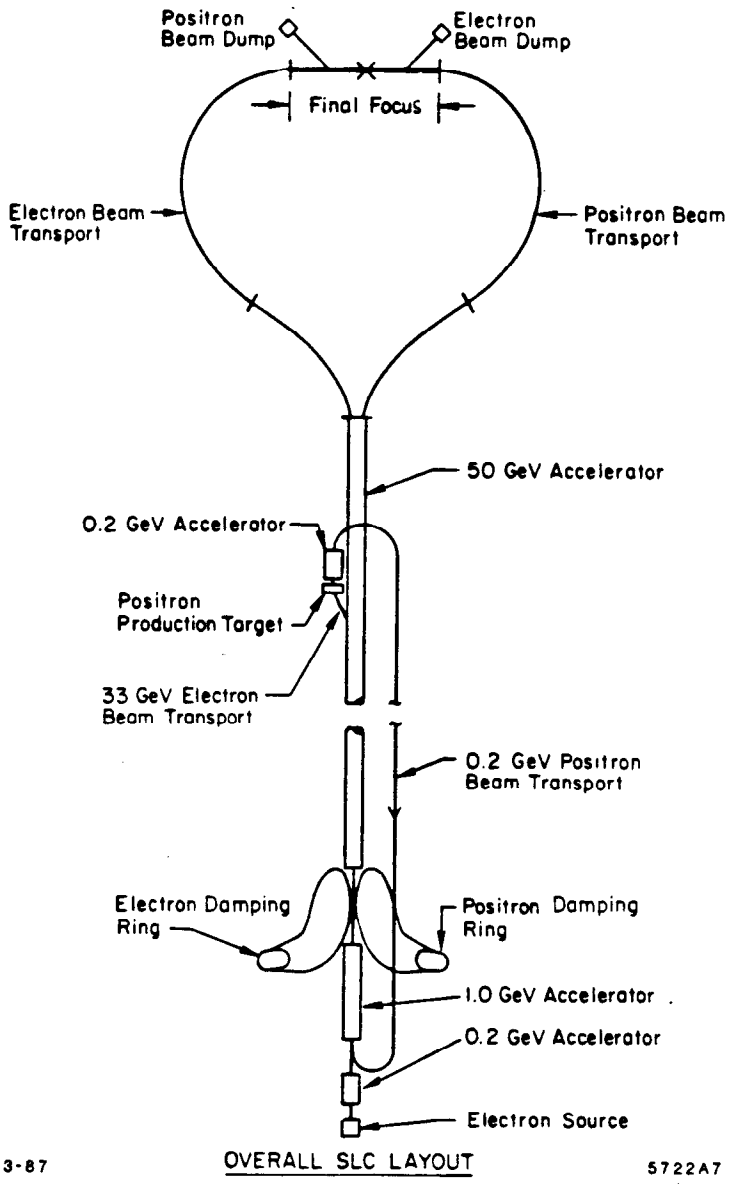

Figure 1 A schematic overview of the Stanford Linear Collider (SLC) (3). The accelerator length, including the arcs and final focus, is about 4 km.

and are reduced to a small size by the final focus system, they are collided at the IP. The spent beams are discarded after a single collision. On the same acceleration cycle, the second electron bunch after being accelerated to about 30 GeV in the linac (2 km) is extracted and made to strike a water cooled tungsten target. Positrons emerge from

the target with energies near 1 MeV/c^2. The positrons are carefully collected while being accelerated to 200 MeV/c^2. They are then transported to the beginning of the linac in a quadrupole lattice (2 km). Upon the arrival of the positron bunch, the first section of the linac (100 m) is pulsed with radio-frequency (RF) power and used to accelerate the positron and two new electron bunches, which are made by either a thermionic or a polarized gun. These bunches are injected into the two 1.15 GeV damping rings, where radiation damping reduces the emittances to values required for small beam sizes at the final focus. Throughout this cycle a second positron bunch has remained in the positron damping ring, where two damping cycles are required to reduce its naturally large emittance. This complete cycle is repeated at 120 Hz. The inherent instabilities of linacs in general have been compensated in the SLC by the use of slow (one minute) and fast (every pulse) feedback systems, all of which are computer driven. Nearly 100 measured beam parameters are actively controlled. In the interaction region the MKII detector was in place from the fall of 1987 through November 1990 (26). The SLD detector is being installed and will be ready for beam by the spring of 1991 (27).

Selected design parameters (28) of the SLC are listed in Table 1. Also included in Table 1 are the best individually achieved parameter values (while not maintaining the others), the simultaneously achieved values during the best MKII data collection period, and the projected parameters for collisions with the SLD. In part, the technological challenges of the SLC come from the large range of beam dimensions at various locations in the accelerator. A schematic view of various beam dimensions in different parts of the SLC is shown in Figure 2. For example, the size of the positron beam changes by four orders of magnitude going from just after the production target, through the various systems, and on to the IP in a few milliseconds. Furthermore, the horizontal to vertical size aspect ratio changes from unity to 250 and back, concurrently. Orchestrating this orderly decrease in beam sizes through the various systems and transitions while minimizing undesired emittance growth requires constant vigilance. The strong focusing quadrupole lattices throughout the collider make this possible to a large degree. A particle that has a transverse displacement of one beam radius, say 300 μm, just after the damping ring will be displaced at the IP 4 km downstream by at most one radius (3 μm) (if we ignore transverse wakefields for the moment) and will remain in collision.

Table 1 SLC accelerator parameters

Accelerator parameter	Units	1984 Design	Best independently achieved	Simultaneous during MKII collisions	Goal for SLD collisions
Beam energy	GeV	50	53	46.6	46.6
Repetition rate	Hz	180	120	120	120
Energy spectrum	%	0.25	0.2	0.3	0.3
N^- at IP	10^{10}	7.2	3.3	2.7	5.0
N^+ at IP	10^{10}	7.2	1.9	1.6	4.0
N^- in linac	10^{10}	7.2	5.3	3.8	6.0
N^+ in linac	10^{10}	7.2	3.5	2.1	5.0
N^- (210 MeV)	10^{10}	8.0	7.0	4.5	8.0
N^+ (210 MeV)	10^{10}	14.0	10.0	9.0	10.0
Ring damping τ_x	msec	3.5	3.8	3.8	3.5
Target e^+ yield	e^+ / e^-	4.0	4.5	4.0	4.0
$\gamma\varepsilon^+_{x(y)}$ in linac	10^{-5} r-m	3 (3)	2.0 (3.0)	2.1 (3.7)	3.5 (3.5)
$\gamma\varepsilon^-_{x(y)}$ in linac	10^{-5} r-m	3 (3)	4.0 (3.0)	7.5 (3.2)	3.5 (3.5)
$\gamma\varepsilon^{+/-}_x$ at IP	10^{-5} r-m	4.	6.	7.4	5.4
$\gamma\varepsilon^{+/-}_y$ at IP	10^{-5} r-m	3.2	4.	4.4	3.6
IP divergence	μrad	300	275	220	300
IP β^*	mm	5	10	15	5
σ^*_x	μm	2.07	3.0	3.5	2.6
σ^*_y	μm	1.65	2.6	2.7	1.6
Bunch length (σ_z)	mm	0.5-1.5	0.5-12.0	1.0	1.2
Pinch enhancement		2.2	1.0	1.0	1.1
Luminosity	$10^{29}/cm^2$ s	60.0	0.45	0.45	5.0
Luminosity	Z^0 / hr	650.0	4.9	4.9	54.0
Efficiency	%	100	90	25	50
Polarization	%	39	0	0	34

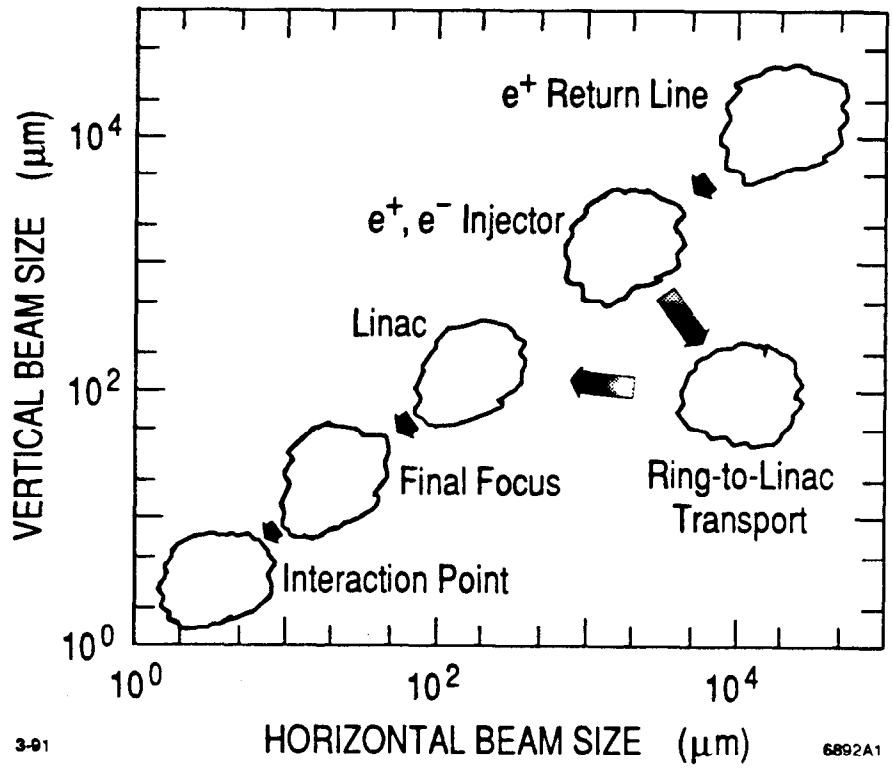

Figure 2 The transverse dimensions of an SLC beam are reduced up to four orders of magnitude from generation through collision. The horizontal to vertical aspect ratio also changes by two orders of magnitude. These variations are routine during operation.

3. ELECTRON AND POSITRON SOURCES

3.1 Electron Source

The electron source (29-31) consists of a 40 MeV injector and a 1.15 GeV, 2856 MHz accelerator. A schematic of the injector is shown in Figure 3. There are two electron guns: one is a thermionic gridded cathode driven by two high voltage pulsers, and the other is a polarized GaAs photoemitter excited by a laser. The polarized source is discussed further in the section 10. The gun must produce two bunches separated by about 60 nsec. After leaving one of these guns, the bunches go through a "Y" bend and into two RF prebunchers operating at 178 MHz. The

prebunchers, combined with the final s-band buncher at 2856 MHz, reduce the 60 cm long 150 keV beam pulse into a 3 mm long 2 MeV bunch through velocity-position correlations. The particle density in these bunches is large, requiring special computer simulation codes (32,33) be used to calculate the expected emittance enlargement from space charge and magnetic transport. The enlargement from the bunching process dominates the emittance generated from the cathode (34). The design of an ideal high current gun remains an active subject. The focus of this research is for future low emittance, high current sources for the next collider and for gun structures for klystrons. Bunch charges over 1.3 x 10^{11} e^- are routinely made with invariant emittances below 5 x 10^{-4} radian-meters (r-m).

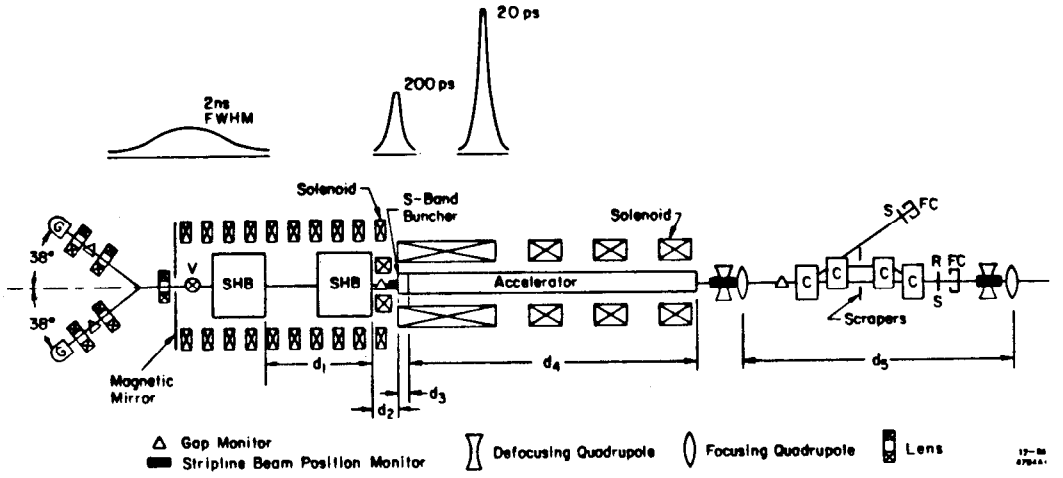

Figure 3 Schematic view of the electron injector showing the thermionic and polarized guns (G), subharmonic bunchers (SHB), s-band buncher, 40 MeV accelerator and energy-analyzing scrapers (30).

After length compression, the two e^- bunches are accelerated in the linac to 210 MeV, where they are joined by the positron bunch coming from the target. These three bunches are then accelerated to 1.15 GeV and injected into their respective damping rings. The intense charge of each bunch requires the compensation of longitudinal beam loading (energy loss) produced by the irises in the RF accelerating structure (35). The phase of each bunch on the RF wave (λ = 10.4 cm) is adjusted to remove the linear part of the head-to-tail internal energy loading. The long-range longitudinal

loading between bunches is compensated by timing changes of the RF so that sufficient refilling of the structure occurs within the bunch separation (60 nsec).

The intense charge in each bunch also requires the control of transverse wakefields which cause off-axis bunches to generate internal forces (36). These forces are such that the longitudinal head of the bunch drives trailing (core and tail) particles to ever increasing amplitudes. There are several methods to control transverse wakefields (see sections 5 and 9). Here, the lattice has short quadrupole spacings, which make a very short focal length to keep the beams near the axis and thus make the response to wakefields smaller. The alignment of the accelerator, quadrupoles, and the beam position monitors (BPM) needs to be at the level of 100 μm (37).

3.2 Positron Source

The positron source (38-40) is designed to produce as many positrons on every pulse as possible so that ultimately the e^+ bunch in its damping ring has as much charge as its electron partner does in the other ring. The process is as follows. The third accelerated bunch (30 GeV e^-) in the main linac is extracted, passed through an extraction transport line, and made to strike a target. Emerging from the target, which is made of tungsten-rhenium and is six radiation lengths long, is a vast spectrum of low energy electrons, positrons, and photons. A portion of the positron spectrum is carefully focused by a pulsed solenoid (flux concentrator) (41) just downstream of the target, accelerated, and bunched by a 1.4-m "capture" accelerator with a gradient of 40 MeV/m (42). The energy of the positron bunch is then raised to 210 MeV in the "booster region" where upon it enters the return line to be transported back to the injector linac 2 km upstream. Internal to the booster region, the particle charge is collimated to remove unwanted captured electrons. After the positrons reach 210 MeV, transverse and energy collimators remove particles that are far off-axis and far off-energy. At this point the positron yield (number of 210 MeV e^+ per number of incident 30 GeV e^-) has been measured to be 2.5, as expected.

The most difficult task in building the positron source has been to design a target that does not crack under intense high power incident bunches. Each 30 GeV electron bunch at 6×10^{10}, with dimensions 0.3 mm diameter and 1 mm bunch length (gaussian sigma), contains 290 joules. Much of this energy is absorbed in the target in a few picoseconds and the rest is absorbed in components downstream. The incoming beam diameter has been enlarged by a factor of two by using a scattering foil a meter

in front of the target . Without the foil the electromagnetic shower from the beam would have a small volume and heat the target to above the temperature where the pressure shock cracks the material in a single pulse. The remaining problem is the average power deposition of the beam arriving at 120 Hz. Many solutions to the heating problem have been studied. The best solution is to make a transversely rotating target that distributes the load evenly over a 2-cm circle. The engineering required to make this device reliable in the heavy radiation environment was difficult (43,44). For example, a nearly automatic removal system was built with quick cable and vacuum disconnects, a remote crane, and special elevator. This remote system can remove a highly radioactive target safely in about one hour with little exposure to personnel (45). Targets for a future collider will use this design as a basis, but an order of magnitude higher beam power is expected.

The length of the positron bunch produced is important because long bunch lengths generate large energy spreads in the injector accelerator that are not accepted easily into the damping ring. A system has been built to monitor bunch lengths by examining the high frequency voltages induced in a cavity through a ceramic window (A. Kulikov, unpublished). This diagnostic device is ideal for a noninvasive length monitor in a potential future collider.

Finally, the positron bunch that is transported to the injector has a large transverse size. The small dodecapole fields in the quadrupole magnets in the return transport line have been shown to enlarge the transverse emittance if the betatron phase advance in the lattice is near ninety degrees per cell (46). Lowering the phase advance per cell improved the emittance, an indication that small errors over many lattice cells can accumulate significantly.

4. DAMPING RINGS

The damping rings of the SLC have been designed to reduce rapidly the transverse emittance of two bunches spaced nearly equally around the 35-m circumference (47-49). In order to make the damping time short compared to the beam cycle time, the horizontal betatron tune ($\nu = 8.3$) was made very high compared with a normal storage ring of that size. As a consequence, the vacuum chamber apertures were made quite restricted to allow for the maximum possible dipole fields (20 kG). Furthermore, the ring is operated on the coupling resonance to make the horizontal and vertical emittances equal. The measured emittance reduction with damping time is as

expected. Even though new lower emittance damping rings have been designed for a next collider and for synchrotron radiation sources, the SLC damping rings have retained the low emittance record for the past decade.

The bunches are injected on axis into the ring using a kicker with a fast fall time (60 nsec) and extracted from the ring a few milliseconds later with a fast rise time kicker (50). The positron ring kickers must have fast rise and fall times so as to not disturb the already stored bunch. The extraction kickers are required to have amplitude stability at the 0.05% level to make the beam trajectory stable in the main linac and thereby avoid transverse wakefields. Furthermore, the timing stability of the kicker pulse must be well below a nanosecond as the kicker pulses do not have perfectly flat tops. The design of these kickers has evolved with time: the latest involves fine control of high power thyratrons, efficient ferrite magnets, radiation hard magnet insulation, subnanosecond timing feedback systems, and perturbative prepulsers (51). This experience will be applied to the next generation collider where tighter tolerances are expected.

The bunch length σ_z in the damping ring is 6 mm at low currents and lengthens toward 10 mm at high currents (52). This length must be reduced to the 0.5 to 1.5 mm needed in the linac. A RF accelerator (32 MeV) operating at the zero phase crossing is located in the ring-to-linac transport line and generates a head-tail energy difference in the bunch. When this difference is combined with the chromatic path length difference designed into the transport line the bunch length is shortened (53). Because of the induced large energy spectrum ($\sigma_E / E = 1\%$) and the resulting beam aspect ratio ($\sigma_x / \sigma_y = 250$), this transport line requires strong corrections to the second order optics, corrections that are made with sextupoles. The transport line was designed using second order achromats in which all the second order chromatic and geometric transport terms were made small (54). This design works well. The concept of second-order achromats is now used worldwide (55). Nevertheless, subtle field errors in the extraction magnets and anomalous magnetic errors in the transport line require first- and second-order betatron, coupling, and dispersion adjustments of the beam at the entrance to the linac.

Transverse instabilities have not been observed in the damping rings, but, three longitudinal effects have: longitudinal bunch lengthening (mentioned above) due to vacuum chamber impedances, longitudinal dipole oscillations (fixed by RF feedback), and coupled bunch longitudinal (π mode) instabilities (56). The π mode instability is temporarily controlled with RF cavity temperature while a feedback cavity

is being designed and built. Studies here apply directly to a future collider in which smaller emittances and larger number of bunches in the damping ring are foreseen.

A jitter of the injection position (x,y) or angle (x',y') into the linac causes wakefield growth and filamentation of the beam during acceleration. The launch jitter comes primarily from amplitude instabilities of sensitive dipole magnets in the damping ring system, including the extraction kicker and septum. Ring trajectory control at the 30 μm level is also needed. Constant improvement of the power supplies has reduced the oscillation amplitudes to their present values: 100 μm horizontally (σ_x / 3) and 30 μm vertically (σ_y / 10) as observed in the linac. The present jitter reduction activities are concentrated on searching for the 0.25 to 0.5 gauss-meters of unstable field with frequencies below 10 Hz and on applying pulse-by-pulse feedback to the launch variables. Field stabilization and rapid feedback are necessities of all future colliders and storage rings.

5. LINEAR ACCELERATOR

The main linear accelerator at Stanford has a length of 2946 m and is powered by 230 klystrons (57). The accelerating gradient is about 20 MeV/m. A strong focusing lattice consists of 282 quadrupoles used to maintain the transverse beam size. A pair of x-y correction dipoles and a stripline beam position monitor are associated with each quadrupole for trajectory correction. High resolution profile monitors, both screen (video) and wire scanners types, are located along the linac approximately every factor of three in energy. Monitors for the energy, energy spectrum, and emittance enlargement are placed near the end of the linac to allow either automatic or operator correction during SLC operations.

The primary goal of the linac is to transform the six dimensional phase-space volume of a low emittance, low energy bunch to high energy without significant phase-space enlargement. Acceleration by itself reduces the absolute emittance of the bunches by increasing the longitudinal velocities of the particles while leaving the transverse velocities constant. However, deleterious effects such as transverse wakefields, RF deflections, chromatic filamentation, and injection errors can increase the emittance, if unchecked. A technique called BNS damping (58) is used to reduce the effects of transverse wakefields: one adds a head-tail energy spread along a bunch by back-phasing early klystrons and forward-phasing later klystrons. BNS damping works very well . More details of these techniques are discussed in the section 9.

The klystrons are the key to acceleration (59). Each produces 67 MW at 2856 MHz for 3.5 μsec. The power is compressed using a SLED system (60). The power is then evenly divided among four 3-m constant gradient accelerating sections on a support girder. At 20 MeV/m, each klystron is thus capable of providing 250 MeV to each particle. The phase and amplitude of each klystron are monitored and adjusted using a new control system that maintains the phase and power tolerances at 0.2 degrees and 0.2% respectively over the 3-km linac length (61). The phase of each klystron can be determined to about 4 degrees absolute and remains close to the desired value for months. The rate at which each klystron produces an errant pulse is well below one for every 10,000 pulses on the average. Thus, at 120 Hz with 230 klystrons, errant acceleration cycles occur well below one every three pulses (about one each second). The mean klystron lifetime is well over 20,000 hours, meaning one klystron each week of operation needs replacement. Finally, a power limitation in the modulators restricts the repetition rate to 120 Hz.

The energy spectrum of a bunch is determined by its current, its bunch length, and the RF parameters. Intrabunch longitudinal wakefields cause a longitudinal position-dependent deceleration, which is mostly cancelled by moving the average phase of the bunch ahead of the voltage crest of the RF wave. For example, at 5 X 10^{10} particles and a bunch length of 1 mm, the tail is decelerated by 2 GeV. A compensated energy spectrum has a complex shape, as shown in Figure 4. Both spectra have widths less than 0.2% rms when 1% energy collimation is made. The "double horned" spectrum at high bunch intensities results from the nonlinear longitudinal wakefields and the curvature of the RF waveform (62). The energy spectra are measured in an energy dispersive region at the beginning of the arcs in a location where the betatron function is low. A noninteracting spectrum monitor (63) has been built using a vertical wiggler magnet to generate a vertical synchrotron radiation stripe (3 MeV critical energy). The x-ray stripe strikes an off-axis fluorescent screen viewed by a video camera. The width of the stripe is a measure of the spectrum. A resolution of 0.07% is routine. Measured energies and spectra versus overall linac RF phase are shown in Figure 5.

With the spectra of both positron and electron bunches adjusted using their respective overall linac phases, the energies of the two bunches are set to the desired values. First, the SLED timing is used to fix the proper energy difference between bunches, and then the appropriate number of klystrons are applied to make the energy

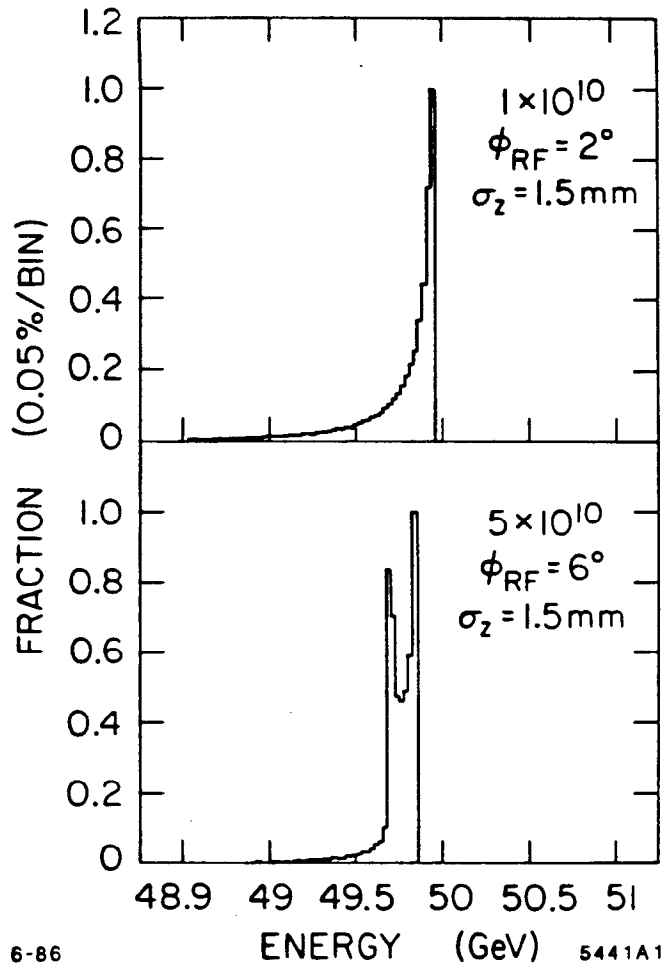

Figure 4 Simulated energy spectrum of a bunch at the end of the linac (47 GeV) at low and high intensities (57). At high intensity the nonlinearity in the RF field and the longitudinal wakefields create the complex shape.

sum correct (64). Examples of the RF and timing parameters needed to make the energies and spectra of the three bunches correct are shown in Table 2 for equal currents. The absolute energy of the two bunches changes rapidly over time up to a percent or so. A pulse-by-pulse feedback system keeps the electron (and positron) energy fixed using opposite-phase adjustments of two eight klystron 'sectors' in the linac (65). This system works well keeping the rms energy variations at about 0.1%. Energy differences between the bunches grow very slowly and an operator or a slow feedback (minutes) can track them.

Bunch current variations from the injector will cause beam loading changes in the linac, which in turn result in energy errors at the arc entrance and at the target extraction line. This problem is severe enough that at high currents one missing e+

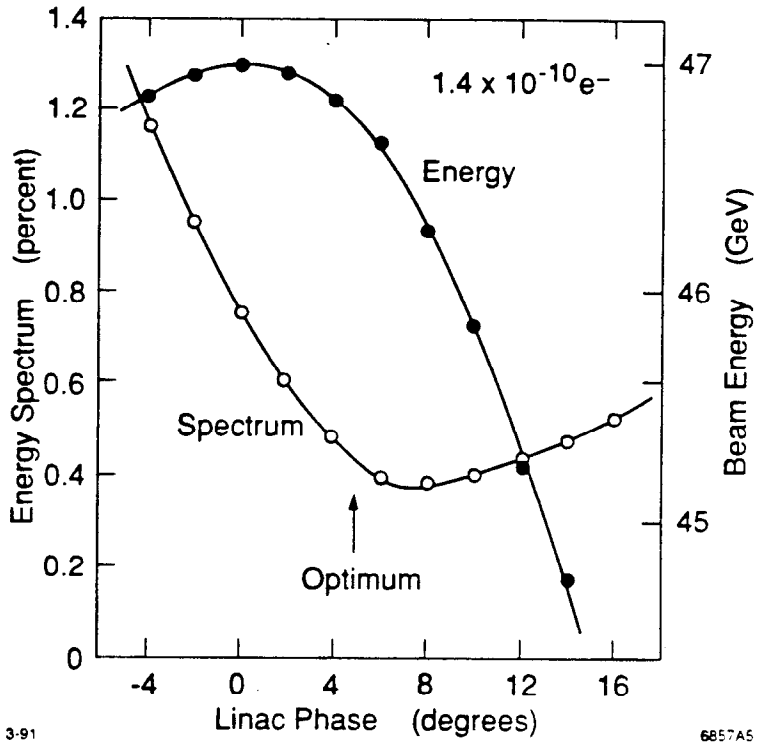

Figure 5 Measured electron energy and spectrum as a function of overall linac RF phase.

Table 2 Multibunch parameters for various beam currents in the SLC Linac at 46.6 GeV average per beam. n_1 (n_2) and ϕ_1 (ϕ_2) refer to the number of klystrons and BNS phase for the linac region upstream (downstream) of the BNS phase change point. The SLED timing refers to the timing placement of the bunches on the RF pulse. A difference in electron and positron energies, with fixed sum, changes the required number of klystrons.

$N^- = N^+$	σ_z	n_1	ϕ_1	n_2	ϕ_2	n_{total}	t SLED	E^- bunch 2	$E^- - E^+$
X 10^{10}	mm	klystrons	degree	klystrons	degree	klystrons	nsec	GeV	MeV
									0
1	0.50	32	-20	160	10	192	- 86	32.6	0
3	0.75	56	-20	152	22	208	- 122	30.5	0
5	1.25	72	-15	136	22	208	- 164	30.6	0
6	1.35	80	-12	127	20	207	- 190	30.7	0
7	1.50	88	-12	124	22	212	- 213	30.3	0
5	1.25	72	-15	132	22	204	- 106	30.5	- 500
5	1.25	72	-15	141	22	213	- 240	30.3	+ 500

- bunch can place the third bunch (e^-) out of the extraction line acceptance and thus stop all future production of positrons. This event is called the "bootstrap" problem, referring to the method of recovery. A fast energy feed-forward system (66) has just been implemented; it measures the current changes in both damping rings and adjusts the klystron phases in an energy feedback system to compensate for the anticipated energy offset in advance of bunch extraction. Lessons learned here are crucial for any future collider, which likely will need many feed-forward systems.

The trajectories of positrons and electrons can be corrected using several steering algorithms (67). Oppositely charged beams can both be steered to nearly the same trajectory even though they are traveling in the same direction because the response of each beam to a given dipole field depends on the betatron function at the dipole. In the lattice, quadrupoles alternate in sign. A given quadrupole focuses horizontally and defocuses vertically; the next magnet is opposite. The corresponding betatron function alternates high to low from focus to defocus quadrupoles and also for oppositely charged beams. The basic unit of this type of correction is called the "magic beam bump' (68). The steering algorithm that works best in the linac is called "one-to-one" in which the electrons are steered to the centers of the position monitors in their focusing quadrupoles and the positrons are steered to their focusing quadrupoles, thus using alternate magnets and position monitors. This algorithm has been shown to be more robust than others against an occasional broken corrector or position monitor. Finally, using a computer program similar to that for trajectory correction, a measured beam oscillation can be used to check and diagnose errors in the lattice phase advance or the local beam energy.

The alignment of the accelerator is important for maintaining the beam emittances. The accelerator structure is supported on girders 12 m long and aligned with a laser system (69). Internal to the girder, the components are aligned using a local optical telescope. In addition, trajectory measurements for both beams using several quadrupole lattice settings are used to make a beam-based determination of the offsets (70). These determinations result in a more accurate check on the alignment than is now possible by mechanical means. Using these methods in combination, the alignment errors of the quadrupoles have been reduced to about 100 microns rms, the position monitors to about 75 microns, and the accelerating structure about 250 microns. Only large earthquakes affect the linac alignment. The California earthquake of October 1989 (magnitude 7.3) produced a 1-cm transverse offset in the linac tunnel

housing, shearing the east half of SLAC from the west (71), see Figure 6. A gentle s-bend over 200 meters was placed in the linac to correct for this shear. The effect on the emittances from this gentle bend are negligible. Also, slow settling of the earth surrounding the accelerator requires periodic realignment.

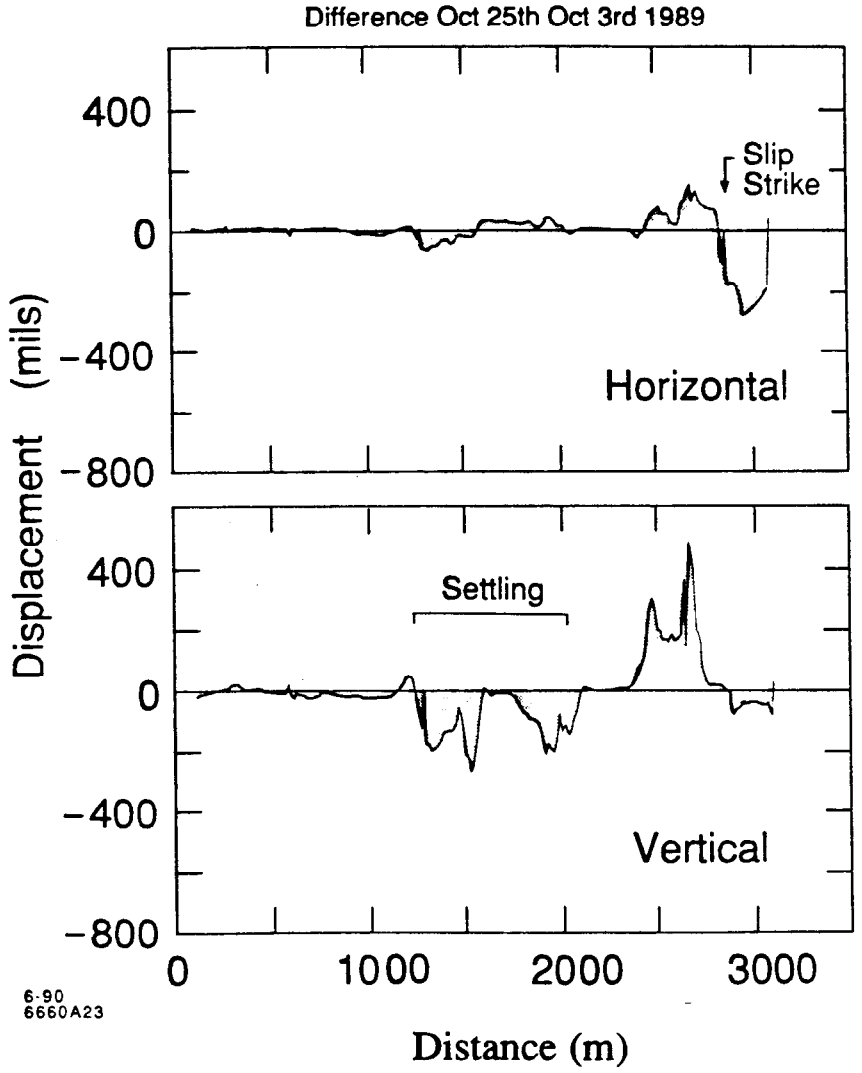

Figure 6 Accelerator misalignment resulting from the October 1989 earthquake.

6. ARC TRANSPORT

The arcs must transport two high energy bunches from the linac to the final focus without significant emittance dilution (72,73). The arc system consists of a short matching region at the end of the linac leading into a very strong focusing FODO array

of combined function magnets including dipole, quadrupole, and sextupole fields. Each lattice cell has a betatron phase advance of 108 degrees and a length of 5 m. Given the length constraints of the site, the arc bending radius had to be 279 m. As a result, each 47 GeV particle loses about 1 GeV to synchrotron radiation in a single pass through the system. Ten pairs of magnets form a second order achromat that can safely transport beams with an energy spectrum of 0.5%. There are 23 [22] achromats in the north [south] arc. At the end of each F [D] magnet within an achromat a beam position monitor is attached to sense the x [y] beam position with an accuracy of about 25 μm. The combined function magnets are moved by motorized jacks for beam steering. To maximize the bending radius, the magnets and the position monitors occupy all of the longitudinal distance, except for a few matching sections.

The existing surface elevation of the SLAC site is irregular so that the arcs were designed to follow the terrain surface. Achromat units (20 magnets) as groups were rotated around the beam axis up to 10 degrees to provide the needed vertical bending. The vertical elevation changes span a range of about 75 feet. The beams easily pass through these rolled transport lines to the final focus. However, there were initial matching problems and slight differences over the length of an achromat of the actual betatron phase advance from the design causing unwanted coupling of vertical and horizontal beam motion at the roll boundaries. Also, slight magnet misalignments contributed. Therefore, unwanted emittance enlargements resulted. A combination of several solutions has now produced acceptable results: tapered rolls at the achromat boundaries, betatron phase corrections using backleg coils on the magnets, trajectory steering by magnet movers, harmonic corrections at certain spatial frequencies, and 3π trajectory bumps (see Figure 7) for skew correction are all distributed where needed along the arcs (74-76). These corrections are made after exhaustive oscillation data are taken throughout the arcs starting in the linac. After measuring the actual first- and (soon) second-order transport matrices R_{ij} and T_{ijk} , one can implement the appropriate corrections. Overall, we learned that with such adjustments and the current knowledge of achromatic systems, terrain following accelerators can be made to work, should they be necessary because of limited funds or difficult terrain.

The sextupole fields in the magnets introduce strong nonlinearities to beam transport if misalignments of the arc magnets are too large. Complex surveying procedures have been devised to align these three dimensionally undulating arcs to a precision of about 150 μm (77). Here also, beam based alignment studies can resolve offsets; for example, those made by the motion of the tunnel floor.

Several emittance increases are unavoidable in the arcs. The emittance excitation from synchrotron radiation is kept to a minimum by reducing the horizontal dispersion function to about 35 mm using the compactness of combined function magnets. The expected emittance growths are $\Delta\gamma\varepsilon = 1.3 \times 10^{-5}$ r-m horizontally and 0.5×10^{-5} r-m vertically at 50 GeV. The vertical enlargement comes from the twisted achromats in the arcs. Several other effects introduce small emittance enlargements. Resistive wall wakefields increase the emittance by a few percent given the bunch charge, shape, and the small vacuum chamber diameter (12 mm) (78). Centrifugal forces from the bunches bending away from their electromagnetic fields also add a few percent (79). Radiation antidamping adds a few percent, as well. All these emittance studies of the SLC arcs are relevant to a future collider, in which two bunch-length-compression sections are likely to be needed (80). These sections must bend high energy, very low emittance bunches through large angles.

In the arcs, misdirected beams can damage components quickly, as the beams have small dimensions ($\sigma_x < 100$ μm). These sizes, when combined with the high energy, can place a power of 70 kW in a very small volume of nearby material. Long-term heat dissipation is also a major concern for vacuum chambers, beam collimators, and profile monitoring instruments. Furthermore, the energy deposition in thick material in a single pulse can be large enough to cause shock waves and instantaneous cracking (81). Several solutions for these heating problems have been successful. All sensitive equipment should be shielded by upstream collimation or by an active beam shutoff that measures beam loss. However, single-pulse beam trips make accelerator operation difficult; an average over several pulses is better, if possible. Thin spoilers are used to scatter the high power beam so that the energy density is much lower downstream in a high power absorbing device, such as a collimator. Finally, average heating losses can be removed by appropriately designed cooling circuits.

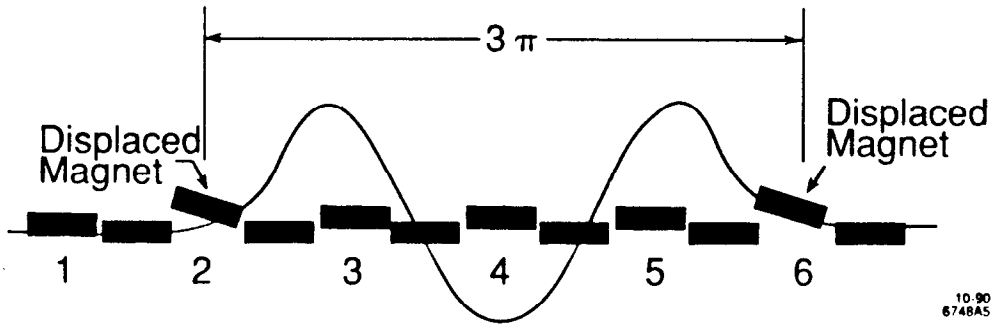

Figure 7 Arc magnet bump using movers for optical skew correction.

7. FINAL FOCUS

The final focus system of the SLC must perform four functions: it must focus the two opposing beams to small sizes at the collision point, it must steer the two beams into head on collision, it must collimate and mask errant particles and synchrotron radiation to make acceptable detector backgrounds, and it must safely transport the disrupted 70 kW beams to respective dumps (82-85).

A schematic layout of the components of one arm of the final focus is shown in Figure 8. The beam first enters a correction region to remove dispersion entering from upstream. Then the beam passes through the first demagnifying telescope where the x and y planes have demagnifications of 8.5 and 3.1, respectively. Betatron mismatches and x-y coupling arriving from upstream are also corrected in this region. Next, the chromatic correction section, which contains gentle bends and sextupoles, is used to correct the trajectories of different energy particles so that they focus at the same longitudinal position at the interaction point (IP). The final telescope provides the last demagnification to make the smallest spots possible and to make the vertical and horizontal spots of equal size. After passing through the IP, each beam traverses through the opposing beam's transport and is deflected into an extraction line to a high power dump. The final focus as built for the MKII detector used conventional iron quadrupoles as the final triplet near the IP. These magnets raised the minimum possible β^* that could be produced because the distance from the IP to the first quadrupole was increased. New superconducting quadrupoles are being installed with the SLD detector (86). These quadrupoles are closer to the IP, which allows a reduced β^* and a doubling of the achievable luminosity.

The minimum spot sizes at the IP depend on the incoming beam emittances, the maximum allowed divergence angles at the IP, and chromatic corrections. The design values for the incoming beam emittances ($\gamma\varepsilon$) are 4.5×10^{-5} r-m horizontally and 3.5×10^{-5} r-m vertically. However, during current operation the actual emittances are about 35% higher. The angular divergence is limited by synchrotron radiation coming from the strong focusing quadrupoles near the IP. The masking near the detector limits the angular divergence to 250 μrad for the MKII and 300 μrad for the SLD. Finally, the chromatic corrections (87,88) are made by eliminating the unwanted first-, second-, and third-order matrix elements: R_{ij} , T_{ijk}, U_{ijkl} , respectively, where the subscripts (1, 2,..., 6) refer respectively to (x, x', y, y', Δl, ΔE/E).

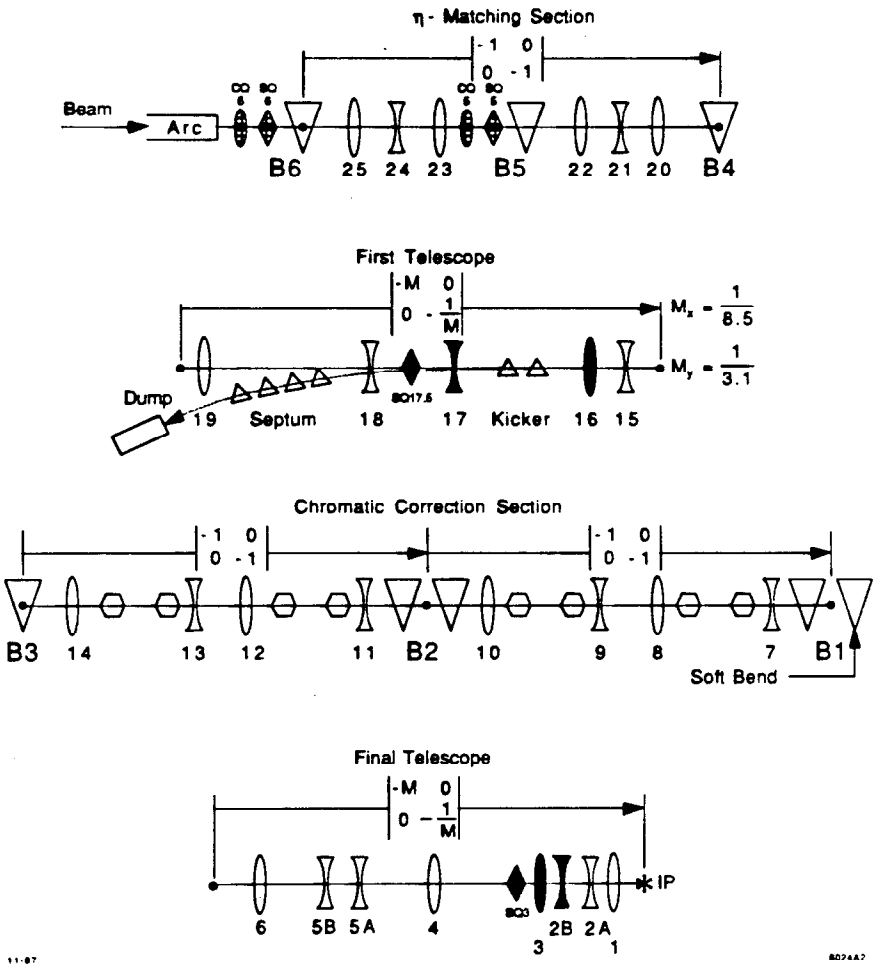

Figure 8 A schematic view of one arm of the final focus system (83). The various sections from top to bottom match the beam phase space from the arcs to the interaction point (IP), demagnify the beam dimensions, and chromatically correct the focusing of off-energy particles.

Chromatic corrections are accomplished by carefully designed symmetries in the final focus. Here are several examples. The first order dispersions (R_{16} and R_{36}) are corrected by placing the final focus dipole magnets in equal strength pairs 180 degrees apart in betatron space. The second order dispersions (T_{166} and T_{266}) are corrected by providing two identical bending modules that have identical dispersion functions but out-of-phase betatron trajectories. The elements (T_{126} and T_{346}) are corrected by using four sextupole pairs in the energy dispersive regions. After the first- and second-order terms are corrected, the third order terms dominate. By adjusting the ratio of the dipole to sextupole strengths in inverse proportion, one can minimize the third order

terms without changing the second-order correction. The best expected spot sizes for the SLC after these corrections are made are shown in Figure 9 as a function of the first order betatron function β^* at the IP. In the actual accelerator these matrix terms must be minimized by real time adjustments. Effective, though elaborate, tuning procedures have been developed for this minimization (88).

The art of chromatic correction presents a challenge for the SLC and especially for a next collider. The new effects of asymmetric emittances, large energy spreads σ_E/E, large angular divergences, energy loss from synchrotron radiation in strong quadrupoles (89), multiple bunches, wakefield steering, and high power density beams have all led to innovative designs, one of which will be tested in the "Final Focus Test Beam" at SLAC (D. Burke, unpublished (1990)).

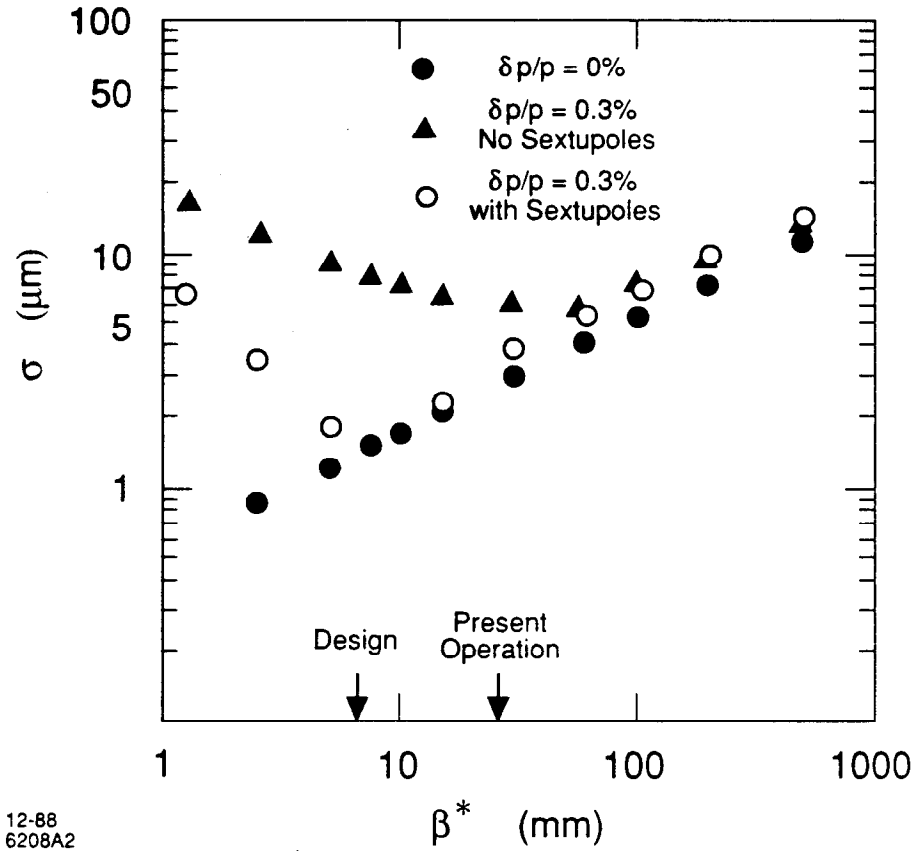

Figure 9 The beam spot size $\sigma(\mu m)$ at the interaction point as a function of the linear optics β^* at the collision point (87). The solid circles represent the sizes produced if only first-order optics are calculated. If second- and third-order optics are included, the triangles are obtained. With the use of sextupoles in the final focus to correct the higher order terms, the open circles represent the improvement in the minimum size.

The beams are very dense at the collision point and can exert large transverse forces on each other, referred to as beam-beam deflections (90). As the two beams are steered through each other, the beam-beam deflection first adds and then subtracts from the bending angle. An example of a measured beam-beam deflection is shown in Figure 10. Beam-beam deflections can be measured in the horizontal, vertical, and skew planes. From the observed deflections, many beam properties can be derived. The beam centroid offsets are determined from the place where the deflection crosses zero. This offset is removed by using nearby dipole magnets to bring the beams into head on collision. The shape of the deflection curve indicates the size of the combined two-beam system and is a good indicator when upstream components have changed the beam parameters. Jitter in the deflection measurements often indicates pulse-by-pulse position changes. Present jitter is about one third of the beam size, and results in only a small loss in average luminosity.

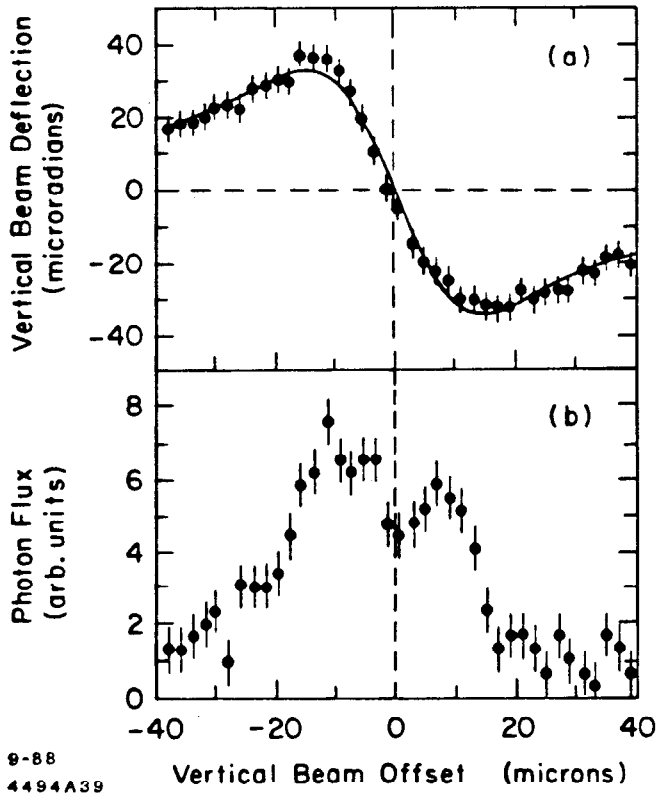

Figure 10 Observed beam-beam deflections at the interaction point are shown in the upper plot (90), and a beamstrahlung radiation signal (radiated photons from the beam-beam interaction) is shown in the lower plot (91).

The particles bent in the beam-beam interaction radiate a form of synchrotron radiation called "beamstrahlung" (91). This radiation travels forward and is detected using a gas Cerenkov detector about 40 m downstream. The radiation from one beam is most intense where the particle density of the other beam is changing most rapidly, at about one transverse beam sigma. The integrated signal over the bunch can be measured as the beams are steered through each other. An SLC beamstrahlung measurement is shown in Figure 10. The signal shape can have a single peak or two peaks, depending on the initial sizes of the two beams. An on-line computer determination of the inferred spot shapes from the beamstrahlung measurements will soon be tested (92).

An exciting feature of the beam-beam interaction is that the beams will focus each other. This mutual focusing is characterized by a parameter called disruption D (93).

$$D = N r_e \sigma_z / \gamma \sigma_x^2 \qquad 2$$

for round beams, where r_e is the classical electron radius. With strong disruption the beams can be markedly pinched over the length of the bunch and result in an increased luminosity. There are many additional effects of disruption: mutual alignment of the beams, kink instabilities, pair production backgrounds from photon interaction with the opposing bunch, and necessarily large outgoing chamber apertures. Disruption plays a major role in the design of the next linear collider. The SLC will not see significant disruption effects until the bunch densities at the IP increase by about a factor of two over the present values.

Collimation of errant particles generated upstream and synchrotron radiation from the final focus quadrupoles has been difficult for the SLC. The aim was to provide backgrounds similar to circular storage rings. However, equilibrium conditions in a ring are much less noisy than transient conditions in a linear collider. Significant progress has been made (94) through many separate contributions. The general collimation system is illustrated in Figure 11. Collimation, both primary and secondary, of particles with transverse offsets are made at 47 GeV at the end of the linac. Both beams pass through eight 1-mm^2 holes spaced over 150 m with only 10 to 20% losses. Just downstream, the off-energy particles are collimated in a dispersive region early in the arcs. Internal to the arcs and in the early final focus there are tertiary collimators for transverse particle offsets coming primarily from scattering from the edges of upstream collimators. In the final focus there is also a secondary energy cut.

Several masks near the detector shield the IP from locally generated synchrotron radiation emanating from the final focus quadrupoles and dipoles. Finally, two magnetized steel toroids on each side of the final focus deflect muons produced in upstream collimators away from the detector. Experience from the SLC indicates that collimation considerations must be dealt with early in the design of a linear collider and that background resistant particle detectors are important.

The energies of the SLC beams are measured very precisely with noninterfering spectrometers in the beam dump lines of the final focus (95). These devices are modeled after the energy spectrum monitor at the end of the linac. Two horizontal dipoles are separated by a precisely known vertical bend. The resulting synchrotron radiation stripes observed downstream are thus separated in angle by the bend of the vertical dipole. Video cameras view the interaction of the radiated x rays with a phosphor coated screen. The image is then digitized and analyzed. These noninterfering x-ray monitors have been very useful, and a future machine will use them extensively.

Since the two colliding bunches take different paths from the linac to the final focus, it is not obvious that the magnetic path lengths can be adjusted accurately enough to center the longitudinal collision point in the final focus. The bunches can be moved relative to each other in the linac but only in steps of one or more complete RF wavelengths (10.4 cm). There is some adjustment in the focal length of the final quadrupoles. However, the larger the adjustment the more difficult the overall operation of the final focus will be. A test of the arrival times of the two bunches in the final focus was made using a Cerenkov radiator and a streak camera (R. E. Erickson, et al., unpublished, 1987). The resulting path difference between the two arcs and final foci (1400 m each) was about 1 mm: a triumph for the survey and alignment group and a significant contribution to the ease of operation of the SLC final focus.

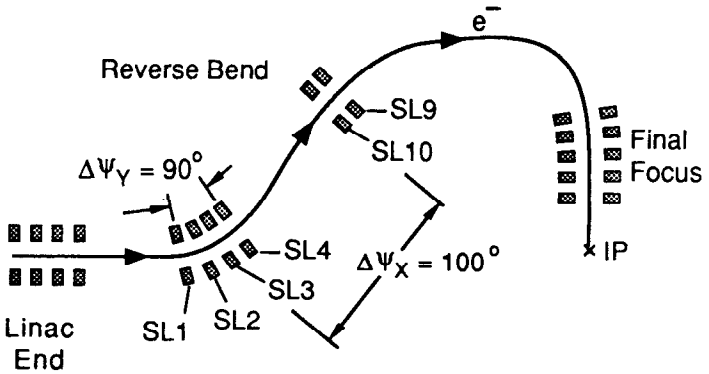

Figure 11 General SLC collimation (e- side). Sixteen movable collimators jaws are located at the end of the linac, 16 in the arcs, and 19 on each side of the final focus.

8. BEAM OBSERVATION AND CONTROL

Control and monitoring of the SLC hardware and beams have significant consequences for stable operations and advancement of accelerator physics. Therefore, a large degree of flexibility has been built into the control system and considerable redundancy into the beam diagnostics.

A VAX mainframe computer interacts through about 75 microcomputers located throughout the accelerator complex to control subunits of the collider (96,97). The microcomputers interact with the hardware through CAMAC hardware, which has sufficient memory and computational power to handle reasonably complicated tasks such as magnet trimming, real-time timing changes to pulsed devices, and the reading and averaging of beam position data. Operators interact with the VAX through control consoles. Each console can operate the entire SLC, and dozens of consoles can be operational at any one time. Reasonable care eliminates most interferences between consoles.

The SLAC linac can in principle produce 360 beam pulses every second (98). The control system allows 256 different beam code definitions, which can be used in any order and at any rate (99). The SLC uses several dozen beam codes to produce colliding beams at 120 Hz. More codes are used for SPEAR, PEP, and nuclear physics beams. With a few new pulsed magnets, all beams could run simultaneously in a time sharing mode. Pulsed devices can be controlled with a timing resolution of about 0.5 nsec. At 120 Hz the accelerator acts differently for the two kinds of beam pulses placed oppositely on the 60 Hz AC line, which is somewhat asymmetric. Pulsed devices and these flexible beam codes allow correction of most of the "time-slot separation" effects (100).

There are approximately 3000 magnets in the SLC. They are calibrated, standardized, and then set to the desired field strengths using field-current polynomials. Several magnets in the damping ring, arcs, and final focus require regulation at the level of one part in ten thousand. When the beam energy changes - for example, when the linac klystron population changes or the experimenters request a different IP energy - the magnets are scaled appropriately. Because the klystron population changes often, the linac magnets are scaled by a special application code that allows completion in well under a minute, including operator interaction.

The VAX computer has several "watch dog" functions in operation constantly to monitor magnets, klystron phases and amplitudes, temperatures, beam trajectories, and total beam pulses. It alerts the operations staff immediately if a parameter exceeds its tolerances. A long term history (weeks) of these parameters is available for study.

Beam position monitors (BPM) are stripline devices with four electrodes (101). The signal from each electrode is sent through a cable to an electronic digitizer, where the position is determined by subtracting the voltage of opposite electrodes and dividing by the sum for normalization. The subtraction is sometimes done before and sometimes after digitization. There are eight different designs for the 2000 BPMs located throughout the SLC, tailored to the local beam properties: for example, high order mode heating must be reduced in the damping ring, centering ability is important in the linac, good accuracy is desired in the arcs, and large diameter and two beam capability are needed in the final focus. The range of resolutions of the BPMs is 10 to 30 microns, limited mostly by digitization. Averaging of multiple beam pulses improves the resolution by a factor of two to three.

The two types of beam profile monitors used most often in the SLC are phosphor-coated screens viewed by video cameras (102) and wire scanners (103). Screen profile monitors place relatively thick plates (100 to 500 μm) into the beam. The plates interfere with downstream operation, but they are very useful in observing real time shape changes and providing detailed information of transverse tail formation. The emittance of a beam can be measured using a screen profile monitor and an adjustable quadrupole upstream. Emittance resolutions of about $\Delta\varepsilon = 1 \times 10^{-10}$ r-m (absolute) are routine. Screen profile monitors were irreplaceable during the early commissioning phase of the SLC when beam jitter and asymmetrical beam shapes occurred frequently. However, with the need for a finer resolution and observed damage to the screen material with higher density beams, wire scanning monitors were developed. Wire scanning profile monitors are now used throughout the SLC.

In the final focus, thin carbon fibers 4, 7, or 30 μm in diameter can be inserted into the vacuum chamber near the IP (104). The beam is moved over the wire using a dipole. Both a bremsstrahlung signal downstream and a secondary emission signal from the wire are measured. This device works very well, achieving a resolution of about one third the wire diameter. However, two effects limit operation at the IP. Above 1×10^{10} particle per pulse and with beam sizes below 4 μm, the beam density is high enough to break the wire from thermal shock on a single pulse. Calculations (D. Walz, unpublished) gave predictions of that threshold. Beam observations on the

breakage of several wires confirm the calculations to within a factor of two. Secondly, at somewhat lower intensities the fields generated by the beam itself reach the level of ten volts per angstrom and the secondary emission signal changes drastically. The fields from the positron beam pulled electrons out of the wire, even though the beam passes by outside. Fields from the electron bunch also affect the emission. Thus, such carbon filaments can be used only for low current studies. High current studies are limited to beam-beam deflections.

Moving an intense beam over a wire leads to substantial particle loss downstream. Therefore, the wire scanning monitors away from the IP are moving devices that scan a stationary beam. Measurements taken upstream of the collimators at the end of the linac can also be obtained during normal colliding operations. Upstream of the IP, wire diameters of 40 to 100 microns are used. As a wire is moved through the beam, scattered radiation is measured by either a photomultiplier tube or a fast ion chamber on every pulse. Secondary emission signals are too difficult to use because the intense beam introduces a "position monitor" signal as well as an emission signal on the wire that must be carefully filtered. The signal that is scanned over the beam is then digitized and fit to a Gaussian curve. In a typical arrangement, four scanners are located near each other, separated by about 45 degrees in betatron phase. The readings from the four scanners made in sequence can be used to determine the emittance and phase space dimensions of the beam (105). Resolutions of $\Delta\varepsilon = 0.3 \times 10^{-10}$ r-m (absolute) have been achieved with bunches of over 3.5×10^{10} e^- at 120 Hz. A computer-automated program scans the wires at the beginning and end of the linac every half hour and records a history of the measured emittances and phase space dimensions for later diagnosis.

Feedback systems are needed throughout the SLC to keep the naturally unstable beams within acceptable tolerances (106). Several pulse-by-pulse feedback systems (mostly independent of the SLC control system) for energy and position at the end of the linac and for position at the IP were commissioned several years ago and have been used with excellent results. Recently, a new fast feedback system,which allows the use of hardware of the SLC control system and takes advantage of modern matrix control theory, has been completed (107). It is now being implemented throughout the project and shows great promise for providing a new level of stable beams.

9. EMITTANCE CONTROL

The absolute transverse emittances ε_x and ε_y of the electron [positron] beam just prior to injection into its damping ring are approximately 1.3×10^{-7} r-m [3×10^{-7} r-m]. This emittance must be reduced by a factor of 265 [800] along its path to the IP. As accounted for in the design, the damping rings store the electron [positron] beam for one [two] acceleration cycles making an emittance reduction of a factor of 10 [30]. Acceleration in the linac reduces the absolute emittance a factor of 41 [41]. The arcs and final focus increase the emittance through unavoidable radiation effects by a factor of about 1.5 [1.5]. The goal for the individual SLC systems is to prevent any additional effects from increasing the emittance. There are many possible enlargement effects (108), and the four different SLC systems are affected by them differently.

The equilibrium emittance of the as-built damping rings is smaller than originally designed. A change in the method of chromaticity compensation using permanent magnet sextupoles allowed a modification to the dipoles that gave a reduced equilibrium emittance. Operating with a coupled beam, the output emittance is 0.6 of the design at 120 Hz. The observed bunch lengthening in the ring does not affect the transverse emittance except for a small lengthening of the linac bunch. It also probably moves the threshold for transverse mode coupling to beyond our operating intensity. The longitudinal π mode instability mentioned in the section on damping rings causes unwanted random trajectory changes downstream where there is finite dispersion. A feedback RF cavity is under construction to reduce this unwanted effect. Finally, the extraction septum has very nonlinear fields near the conductor blades, as all septa do. If an extracted beam trajectory is moved toward the septum, the vertical betatron function first becomes mismatched from the extra quadrupole field and later the emittance increases directly from higher order fields (109). Care in the placement of the extracted trajectory is therefore important.

The bunch in the transport line from the ring to the linac is shortened in length by adding a large energy spread, which in turn introduces chromatic focusing effects. First- and second-order matrix elements involving the energy must be properly adjusted or the enlarged beam size entering the linac will undergo filamentation downstream. Quadrupole and sextupole adjustments are required to remove these errors using measured trajectories, emittances, and betatron functions in the early part of the linac as observables. Since the beam aspect ratio in this transport line is as large as 250, small skew quadrupoles are needed to compensate for rotation errors.

In the linear accelerator many emittance enlargement effects may occur: some result from injection errors, some arise from accumulation of errors along the linac, and some occur at the end. The injection errors include betatron mismatches, dispersion mismatches, x-y coupling, static injection offsets, and launch jitter. Accumulating errors include transverse wakefields, misaligned quadrupoles and position monitors, RF deflections, and component vibration. Effects at the end of the linac include collimator wakefields and x-y coupling.

Betatron mismatches occur when the injection bunch has a phase-space orientation (β,α) that does not match the linac lattice (110). The linac lattice cannot be chromatically corrected because it is straight. Therefore, particles with different energies have different oscillation frequencies. Since the injected beam has an internal energy spread that changes during acceleration, the trajectories of the different energy portions of the beam rotate in phase space at different speeds and soon undergo filamentation. Given a beam β ($\alpha_0 = \alpha = 0$) that is mismatched from the lattice design β_0, the emittance enlargement after filamentation is $\varepsilon / \varepsilon_0 = (\beta / \beta_0 + \beta_0 / \beta) / 2$. Standard emittance measurements can give the actual betatron functions of the beam and indicate the corrections needed.

Dispersion mismatches are similar (111,112). A dispersion η error means that there is a transverse position-energy correlation, $x = \eta \, \Delta E / E$. This correlation adds to the apparent size and emittance of the beam: $\sigma^2 = \varepsilon \beta + \eta^2 (\Delta E / E)^2$. Given the chromatic lattice, the beam particles displaced by dispersion undergo filamentation if allowed and the real emittance grows. Minimization of the measured emittance early in the linac, by making carefully specified adjustments to the quadrupoles in the transport line between the damping ring and linac, removes the dispersion (113).

Emittance growth from x-y coupling occurs when particle trajectories in one plane, say x, are rotated into the other plane (y) by skew transport elements such as rotated quadrupoles or off-axis sextupoles (114). This problem is of more concern for a future collider, where flat beams are needed. Coupling can increase both effective emittances (x and y) or move emittance from one plane to the other. Filamentation of the mixed beam can cause further growth.

A static launch error of the beam injected into the linac generates a betatron oscillation. Standard trajectory correction restores the proper launch. However, if the launch of the beam jitters more rapidly than feedback can correct it, other methods of control are needed. The transport equation of motion for various particles in the bunch is used to study oscillations along the linac.

$$\frac{d^2}{ds^2} x(z,s) + k^2(z,s)\, x(z,s) = \frac{r_e}{\gamma(z,s)} \int_z^{\infty} dz'\, \rho(z') W_{\perp}(z'-z)\, x(z',s), \qquad 3$$

where s is the distance along the accelerator; z is the distance internally along the bunch; k is the quadrupole focusing term (which varies along the linac and along the bunch because of energy changes); ρ is the line density; W is the transverse wakefield due to the accelerating structure; and r_e is the classical electron radius. The left-hand side of Equation 3 represents the form of a betatron oscillation including (slow) acceleration. The right-hand side indicates the forces from transverse wakefields on a particle generated by position errors in the accelerating structure of all the preceding particles in the bunch. The transverse wakefields for the SLC structure increase in strength with the distance between the leading and the trailing particles (115). Thus, the particles at the end of the bunch, in general, see the largest forces. The displacements grow exponentially with distance along the linac (116). Photographs of beam transverse enlargement at the end of the linac from betatron oscillations started at the linac entrance using a dipole magnet are shown in Figure 12. In Figure 13 observations clearly show

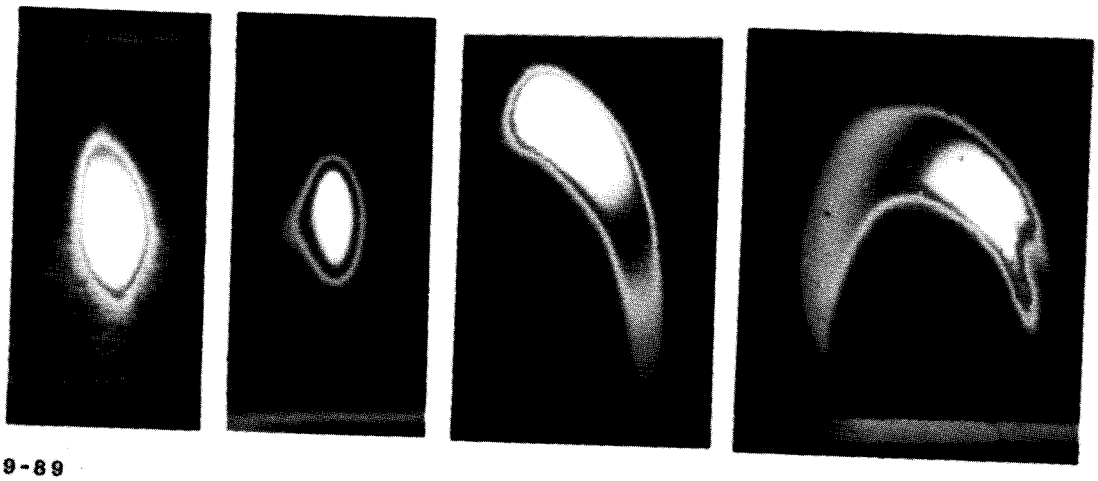

Figure 12 Images of an electron bunch on a profile monitor at 47 GeV showing wakefield growth with increasing oscillation amplitudes (136). The images from left to right are for a well-steered beam, a 0.2 mm oscillation, 0.5 mm oscillation, and a 1.0 mm oscillation, respectively. The beam intensity is 2 X 10^{10} electrons. The core sizes σ_x and σ_y are about 120 μm.

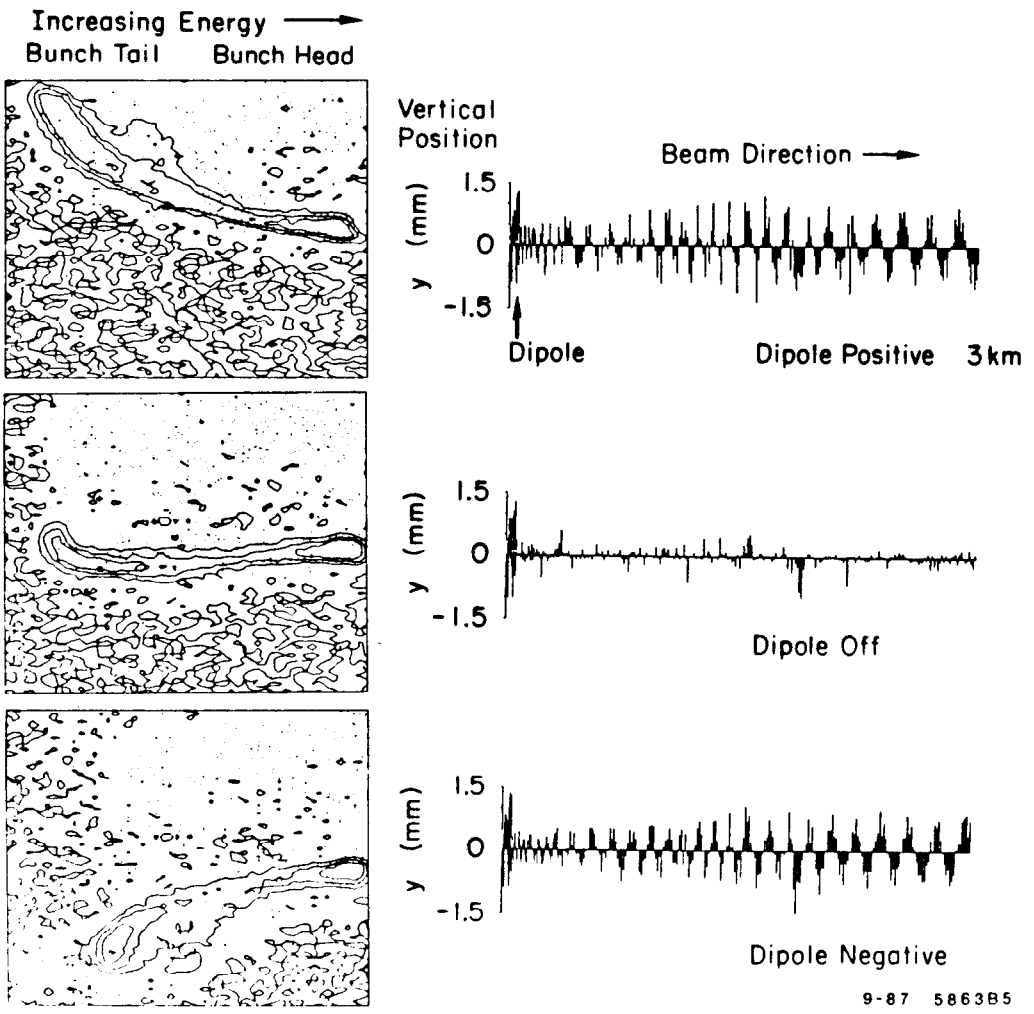

Figure 13 Experimental results demonstrating that the bunch head drives the tail to larger amplitudes during a betatron oscillation due to transverse wakefields (116). On the right side three trajectories (transverse positions along the linac) are shown. The upper plot has a 'positive' oscillation produced by a small change in a dipole magnet early in the linac, the center shows 'no' oscillation, and the bottom a 'negative' oscillation. On the left side the three resulting beam shapes are shown measured on a profile monitor. The accelerator conditions are such that the longitudinal head of the bunch is located on the right side of the measured profile and the longitudinal tail is on the left side. Note that the position of the bunch head is independent of the oscillation but that the tail of the bunch moves vertically with the sign of the oscillation. This example shows that leading particles in a bunch drive trailing particles to large amplitudes via transverse wakefields.

that leading particles which are off-axis in the accelerator excite trailing particles to larger amplitudes. This strongly forced oscillation of the tail by the head (seen in Equation 3) can be ameliorated by changing the energy spectrum along the bunch so that the head is higher in energy than the tail; this can be accomplished with RF phasing adjustments. The wakefield forces, which act like a defocusing force on the tail of the bunch, can be mostly cancelled by the increased focusing of the tail by the quadrupole lattice. This effect is called BNS damping. BNS damping has been studied at the SLC (117) and has been shown to be so effective that all linac operations now use it.

With BNS damping conditions, the oscillations of a bunch can be studied in the linac. Four measured oscillations, with identical initial conditions, are shown in Figure 14 for four different bunch currents. The BNS settings are for 2.5 X 10^{10} particles, where the first 48 klystrons have a phase of -20 degrees and the remaining klystrons have a phase of +15 degrees. In all cases the overall linac phase was adjusted to make the energy spectrum correct at the end of the accelerator. At low current the oscillation decoheres because of the large energy spread. At 2.5 X 10^{10} particles BNS damping is nearly correct because the oscillation damps approximately was the square root of the energy, as expected. At this setting the bunch resists wakefield emittance enlargement. At the highest current the BNS conditions are no longer effective and the oscillation starts to grow exponentially at the end of the linac, similar to the examples in Figure 13. A tolerance on injection position (and angle) jitter can be calculated from this data, with proper BNS conditions at each current. To maintain luminosity, the oscillation must be kept below about $\sigma_{x,y} / 3$ at the end of the linac. The results are shown in Figure 15. At 7.5 X 10^{10} particles, the displacement at the beginning of the linac must be less that 40 μm, within a factor of two of our present operational value. Similar tolerances for a future collider will be significantly smaller, as the emittances are much lower.

The cancellation of wakefield forces by BNS damping may be exploited further. By careful arrangement of the bunch charge density based on knowledge of the local beam energy, lattice, bunch length, and RF structure, nearly all particles in the bunch can be made to follow exactly the same trajectory. The conditions for this behavior can be derived by substituting an identical oscillation into Equation 3 for all particles, and cancelling position terms on both sides (118). This condition is called autophasing (119). However, simulations and experimental attempts to match this special condition in the actual operation of the SLC have not been fruitful to date, though studies continue. If this condition can be satisfied in a future collider, the beam intensity threshold for wakefield emittance growth will increase significantly .

Misalignments of quadrupoles, position monitors, and accelerating structures in the linac cause each beam (after correction) to have a trajectory that is neither straight nor centered in the accelerating structure. These offsets generate dispersion and wakefield emittance growth as described above. There are several methods to deal with these errors. (a) They can be found mechanically and fixed, although the required accuracy is well below 100 μm (120). (b) Calculations using knowledge of the beam trajectory as a function of the quadrupole lattice strength can determine the relative quadrupole and position monitor errors to about 75 to 100 μm (121). The misalignments can then be mechanically corrected. (c) A dispersion reducing trajectory correction may be tried (122). (d) Mechanical movers of the RF structure in the tunnel

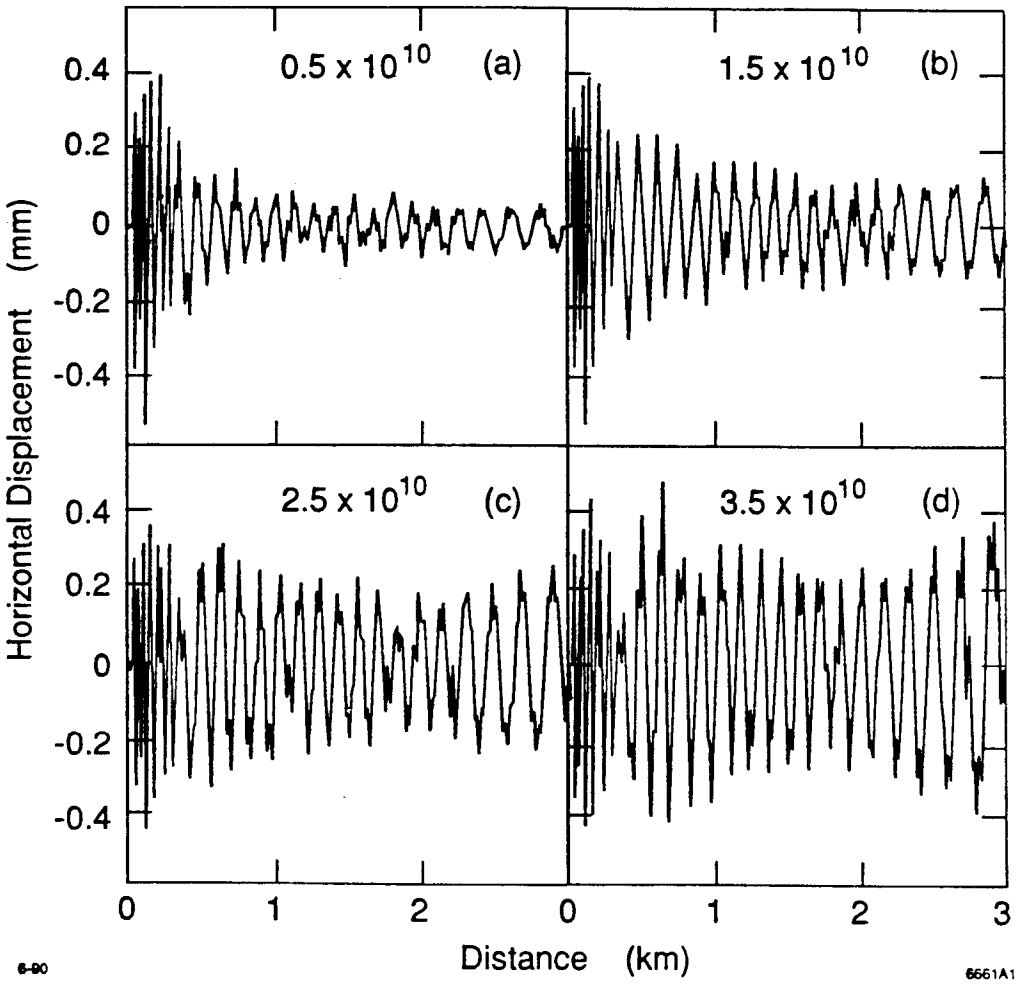

Figure 14 Observed driven single bunch oscillations along the linac versus charge.

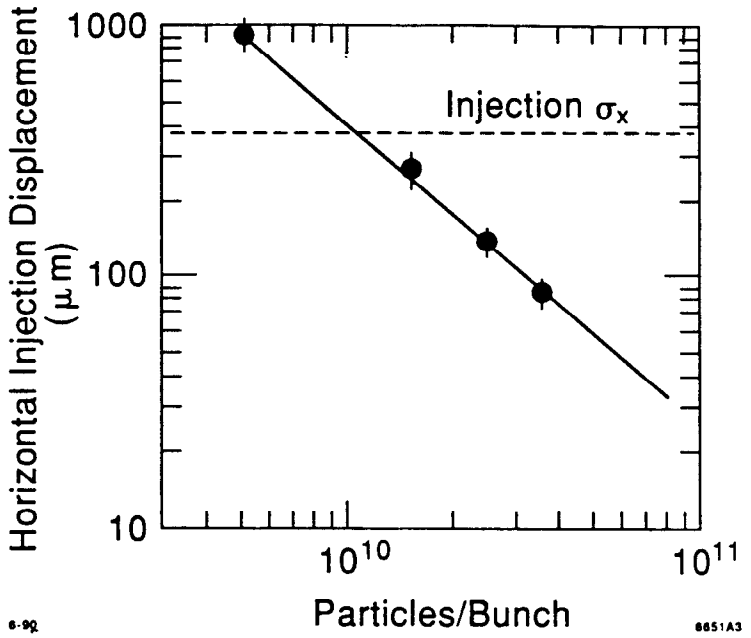

Figure 15 Injection tolerance versus bunch population as measured in the SLC.

can be used in a betatron harmonic correction scheme to reduce the final emittance (123). (e) Betatron oscillations can be forced onto the beam at various locations along the linac to cancel effects of the existing absolute trajectory and thus minimize the final emittance (124). (f) Finally, harmonic changes can be added to the quadrupole lattice to cancel random and systematic errors in the quadrupole field strengths (125). The best combination of the available solutions depends on the particular errors involved. All have been tried on the SLC linac with various degrees of success (126).

The RF structures in the linac have several small asymmetries that generate transverse fields (127). These transverse fields can be in- or out-of-phase with the accelerating fields and deflect (slightly) all or portions of each bunch. The accumulation of these kicks along the linac can enlarge the emittance. There are three effects. (a) The average deflection component can be removed by trajectory correction. However, changes in the RF amplitude of a klystron cause changes in the deflecting fields and thus position jitter downstream (128). (b) The steady state portion of the transverse RF kick causes local trajectory changes, even with steering, and produces off center beams leading to dispersion and wakefield growth (129). (c) Finally, the magnitude of an RF deflection can vary over the length of the bunch, which causes direct emittance growth and further filamentation downstream (130). Care must be taken during construction of

the RF structure to minimize these asymmetries. They cannot be fixed after construction except possibly by cancellation using appropriate pairing.

Mechanical vibration of quadrupoles in the SLC causes trajectory jitter in the beams, resulting in dispersion and wakefield emittance growth. Studies in the SLAC tunnels of quadrupoles with solid supports show vibrations at the 0.05-μm level, mostly with frequencies below 10 Hz (131). Quadrupoles centered on long girders (12 m) show 0.5-μm vibration levels at the resonant frequency of the girder (about 8 Hz) (132). These levels are adequate for the SLC but study is needed for the next collider. Low solid supports may be adequate for most of the next accelerator but active vibration control is needed in the final focus.

The intense small beams at the end of the linac are passed through small collimators to remove unwanted halos. If the core of the bunch is slightly off-axis in these collimators, the bunch experiences deflecting forces that vary over the bunch (133). The SLC conditions are such that this effect is reasonably small. However, for the next collider special collimation sections must be designed (134).

The emittance growth due to radiation from the dipole magnets in the arcs and final focus was minimized in the original design. However, anomalous dispersion and x-y coupling are major effects that are measured and minimized by using the techniques described in their respective sections (135).

In summary, the many studies of emittance in the SLC have made significant progress toward our desired emittance goals, even with increased beam currents. A time evolution of the gains in emittance and beam currents is shown in Figure 16 (136).

10. POLARIZATION

A polarized electron source with a three-electrode photocathode is being prepared for use in late 1991 to provide longitudinally polarized electrons at the IP for a precision measurement of the Weinberg angle ($\sin^2 \theta_W$) (137). The polarized electron bunches are handled exactly the same as unpolarized bunches downstream of the gun, with the exception of injection and extraction from the damping ring. The transport line from the linac to the damping ring is designed to have the proper energy and spin precession angle so that a longitudinal, superconducting solenoid (6.4 Tesla-meter) located in that line rotates the spin into the vertical direction for injection into the ring (138). The vertical spin remains polarized during the damping cycle if care is taken to

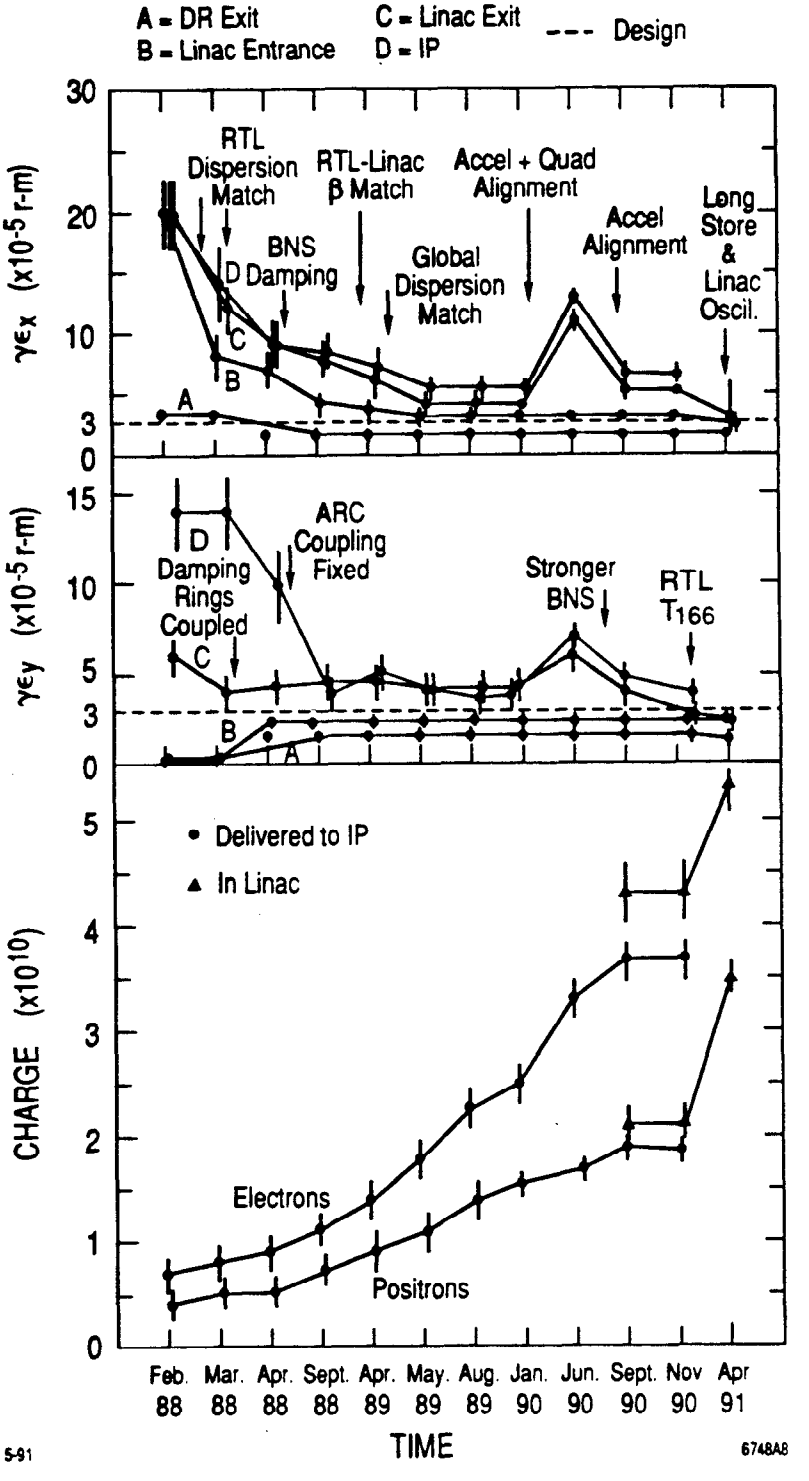

Figure 16 Time evolution of the SLC linac beam emittances and intensities (136) showing when significant corrections occurred. Note the large increase in beam brightness with time. The April 1991 emittances are for 3.5 X 10^{10} electrons.

avoid depolarizing resonances. On extraction, the bunch passes through two similar solenoids, one in the ring-to-linac transport line and the other in the early linac. These solenoids are used to align the spin in the precise orientation to make longitudinally polarized electrons at the IP after many precession cycles, both horizontally and vertically in the SLC arcs. The polarization direction of the electrons from the gun will be changed randomly by 180 degrees pulse-by-pulse in order to remove systematic errors in the data.

The circularly polarized light that irradiates the gun cathode comes from a pulsed dye laser. Pumped by a flash lamp, the dye laser produces about 70 kW of peak power in a 600 nsec pulse at up to 120 Hz. Additional opto-electronic devices will be used to divide this pulse into two 3-nsec micropulses separated by the 60-nsec spacing required by the SLC electron bunches. The stability of the timing and intensity of the light source are important for efficient SLC operation. Tunable solid-state lasers are interesting possibilities for a future upgrade.

A new gun with an improved design is under construction (139). The details are shown in Figure 17. A beam of polarized electrons is emitted from a specially prepared GaAs cathode after a pulsed optical beam illuminates the surface. The GaAs cathode is biased negatively and emits electrons with a quantum efficiency of about 1% and a polarization of 40 to 50%. Gun gap voltages of well over 100 kV are needed to reach SLC single bunch intensities.

There are three polarimeters to allow measurement of the spin direction. One Moller polarimeter is installed at the end of the linac and a second one in the transport line to the electron dump in the final focus. A Compton polarimeter is also installed in the final focus. Even with the often noisy backgrounds of the transient beams in the SLC, these polarimeters have seen clean signal-to-noise ratios and stand ready for the coming of polarized electrons.

The depolarizing effects of the accelerator RF fields in a linac were shown long ago to be small (140). However, with higher gradients and the bunches being off the RF crest because of BNS damping, a new calculation was done (141). Again, the effects were small but nonzero. Since future linear colliders will also use polarization, experimental studies on the SLC are crucial for planning their spin systems.

Studies of new materials for photocathodes that will produce nearly 100% polarization are under active investigation (142). The motivation for a higher polarization is that the effective luminosity for the physics process being studied at the IP is directly proportional to the square of the polarization.

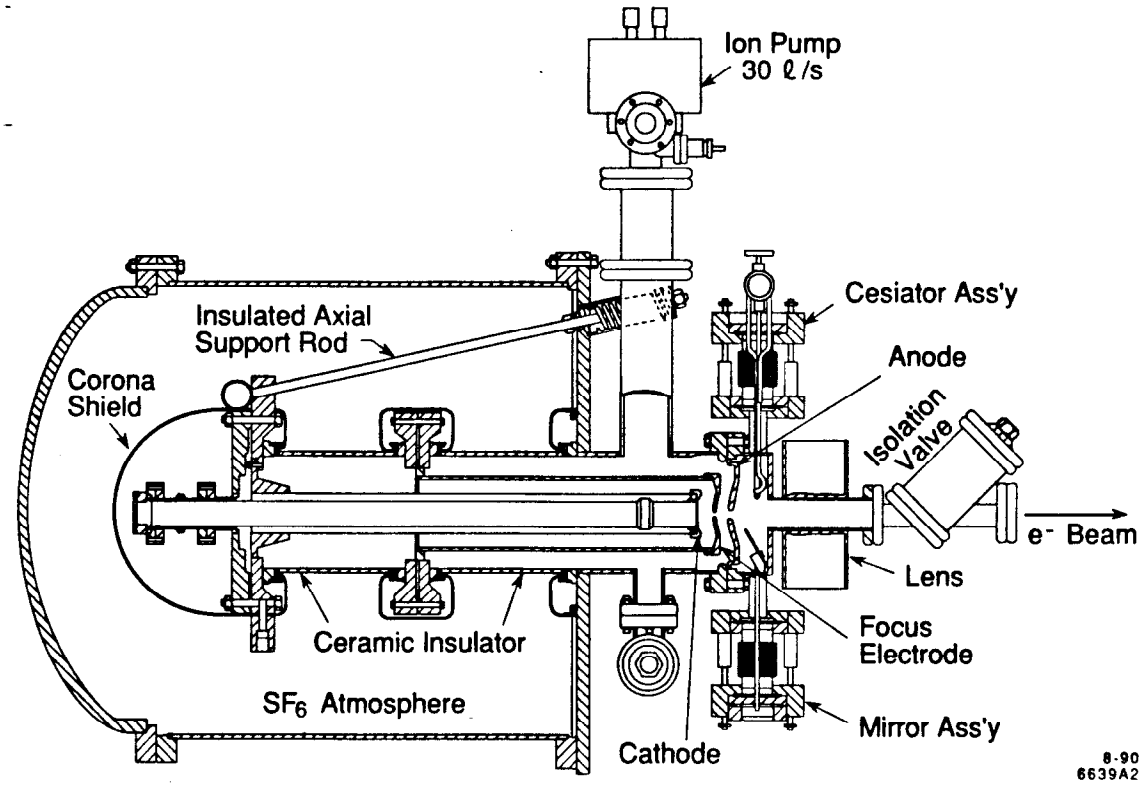

Figure 17 Detailed view of the new SLC polarized electron gun incorporating a GaAs cathode processed with cesium (139).

11. HISTORY, COMMISSIONING, AND RESULTS

The luminosity of the SLC has grown steadily during commissioning and the first collision experiments. The peak instantaneous luminosity recorded over the life of the SLC is shown in Figure 18. The luminosity is determined by (a) measuring separately all the parameters entering Equation 1 and (b) guaranteeing that the beam-beam defections at the interaction point are of the proper magnitude, which indicates centered collisions. The rise in luminosity follows an exponential curve with an e-folding time of about one month for the first period and two months in the past two years. The growth is highly correlated with accelerator physics studies and new hardware (143). Hardware improvements made during the installation periods yielded immediate gains early in the project, but later gains required more commissioning time as the accelerator operations became more involved. In addition, the peak luminosity growth rate decreased with time because the accelerator time was being used extensively for collisions, as it should be.

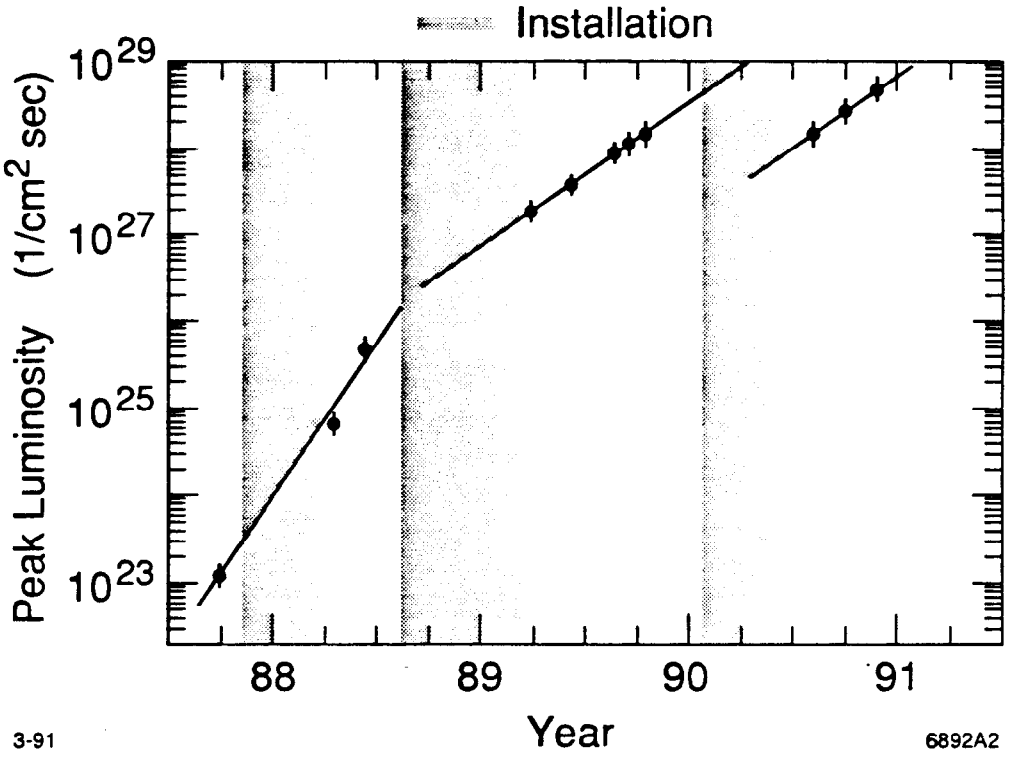

Figure 18 The measured peak luminosity of the SLC over the past three years. Recently, the luminosity has increased at the rate of an order of magnitude for every six months of time devoted to accelerator physics studies (143).

The determination of the expected integrated luminosity from the peak luminosity is complicated by many factors. There are several inefficiencies: (a) The accelerator has downtimes, mostly random, due to broken hardware (10%) and the necessary tuning recovery time afterwards (10%). (b) The luminosity does not remain at its peak because of drifting accelerator parameters requiring active operator intervention (5%). (c) Backgrounds often become too severe from drifting accelerator parameters and require frequent retuning (20%). (It is natural to push the performance of the accelerator until the tuning time is about 25%.) (d) The beams do not remain colliding head-on without active control (5%). (e) The particle physics detector has intrinsic 'dead' time from overlapping events and electronic event readout (20%) and from system-hardware downtime as well (10%). Thus, the overall efficiency compared to the peak luminosity is the product of the efficiencies, or about 40%. This efficiency is comparable with that of other (circular) colliders. (f) Whether to spend time on accelerator physics or on collisions is a difficult decision; collisions add to the Z^0 total

count but accelerator physics studies increase the luminosity. (g) Finally, the number of observed events depends on whether the experimenter has the beam energy set to the peak cross section of the Z^0 resonance or not. In total the SLC has integrated about a thousand Z^0 boson equivalents.

The number of active components in the SLC, including power supplies, klystrons, kickers, vacuum pumps, computers, controls, and instrumentation, is nearly an order of magnitude larger than that of recently built circular electron colliders. Since a very large fraction of these components must be operational in order for the accelerator to function, the reliability of each component must be greater. Much effort is spent at SLAC to maintain reliable active components. A future linear collider, as well as any new large circular collider, will have a still larger number of components. Reliability engineering must be an ongoing study.

12. SUMMARY AND CONCLUSIONS

The Stanford Linear Collider has gone from a conceptual idea to an active research tool in just over a decade. Many new accelerator techniques have been proven on the SLC and some hard realities discovered. The accelerator physics of linear colliders has advanced tremendously. In addition, a high energy physics program explored the properties of the Z^0 boson and continues today with the near-term implementation of polarized electrons to the interaction region.

There have been many accelerator physics successes (too many to discuss them all here). The controlled collision of opposing 3 μm diameter beams, the transport of very low emittance beams, the alignment of the accelerator components at the 100 μm level, and acceleration and energy control of multiple bunches with 0.1% stability are crucial steps towards a next collider. The proven ideas of second order achromats for emittance preservation, the control of 10,000 active devices, and the operation of a 70 kW high-energy-density positron target are also necessary milestones. Advances have been made in the production and transport of polarized electrons in intense bunches. The use of active pulse-by-pulse feedback throughout the accelerator to control over one hundred beam variables is unprecedented. These key steps along with many others achieved at the SLC confidently point towards the design of a future collider.

Several operational issues of the SLC illustrate the unavoidable fact that all large accelerators will have inefficiencies. The SLC is an interrelated complex of smaller

accelerators: injector, damping ring, linac, positron source, arcs, final focus, and physics detector. Each of these subparts has its own difficulties but, nevertheless, must function with a high degree of reliability in order for the whole to operate efficiently. A fault or tuning problem in one system impedes progress in all other systems. The SLC has had its share of difficulties: detector backgrounds from errant particles, kicker reliability, long term maintenance of 25 year old equipment, constant trajectory control, recovery time after a downtime, lack of redundancy in several diagnostic systems, pulse-by-pulse jitter, time pressure, and aggressive schedules for technological advances. Many of these issues of the SLC have been either solved or reduced significantly over the three years of operation. Improvements in the handing of high-power, high-repetition-rate beams remain to be done. Progress has been very steady, although sometimes slow. Overall, no accelerator physics issue has been discovered which prevents our reaching the goals of Table 1.

Finally, here are several general comments on accelerator design and commissioning learned through observations. [1] All potential problems with accelerator operation surmised during the design stage should be thought through carefully, if not acted on, so that a solution can be easily incorporated in the as-built machine. As much flexibility as possible should be incorporated. [2] Commissioning of the subparts of the accelerator should be done in parallel so that all groups can be fully utilized and solutions can be developed in parallel. [3] Accelerator studies must sometimes be attempted even with less than ideal beam conditions so that overall progress can be obtained more rapidly. [4] Most importantly, if a beam problem cannot be measured quantitatively, it cannot be fixed. Beam parameters entering and exiting an accelerator subpart must be measured carefully. The transition regions between accelerator subparts are as important as the repetitive regions within a subpart.

Looking into the future, work is under way at SLAC and around the world to make a detailed design of the next linear collider. Much exciting work remains for this design. The accelerator results and lessons learned from the SLC are playing a key role in shaping realistic plans.

13. ACKNOWLEDGMENTS

The design, construction, and commissioning of the Stanford Linear Collider required the dedication, insight, hard work, and perseverance of many people at the Stanford Linear Accelerator Center and from associated universities and laboratories.

Many technical groups have worked closely together for years to make the SLC a viable accelerator: groups focusing on accelerator physics, operations, controls, instrumentation, vacuum, detector, polarization, mechanical engineering, power conversion, RF engineering, software, and facilities. Also, many visitors from around the world have contributed to the SLC. It is to the credit of the over 1000 people involved that tremendous progress has been made in understanding the theoretical and experimental accelerator physics needed for linear colliders and that the first observations of the hadronic decays of the Z^0 boson were completed. M. Platt helped edit this document.

14. REFERENCES

1. Stanford Linear Accelerator Center, *SLAC Linear Collider Conceptual Design Report*, SLAC-Report-229, Stanford: SLAC (1980)
2. Richter, B., *Proc. of 11th Int. Conf. on High Energy Accel.*, ed. W. S. Newman, Geneva, Birkhauser Verlag: 168-188 (1980)
3. Erickson, R., ed. *SLC Design Handbook*. Stanford: SLAC (1984)
4. Ecklund, S., *IEEE Trans. Nucl. Sci.* NS-32: 1592-1595 (1985)
5. Stiening, R., *IEEE Trans. Nucl. Sci.* 87CH2387-9: 1-7 (1987)
6. Sheppard, J., *Proc. 2nd Int. Workshop on Next Generation Linear Collider*, Tsukuba, KEK Report 90-22: 1-34 (1990).
7. Seeman, J. T., *Proc. of 1990 Linear Accel. Conf.*, ed. C. Beckmann, Los Alamos Nat. Lab., Report LA-12004-C: 3-7 (1990)
8. Wilson, P., In *Proc. of 1988 Linear Accel. Conf.*, ed. C. Leemann, CEBAF-Report-89-001: 700-705 (1988)
9. Guignard,G., In *Proc. of 1990 Linear Accel Conf.*, Los Alamos Nat. Lab., Report LA-12004-C: 8-12 (1990)
10. Takata, K., *Proc. of 1990 Linear Accel. Conf.*, Los Alamos Nat. Lab., Report LA-12004-C: 13-17 (1990)
11. Skrinsky, A., In *Proc. 12th Int. Conf. on High Energy Accel.*, ed. F. T. Cole, R. Donaldson. p. 104. Batavia, Ill: Fermi Natl. Accel. Lab. (1983)
12. Siemann, R. H., *Annu. Rev. Nucl. Part. Sci.* 37: 243-266 (1987)
13. Seeman, J. T., *IEEE Trans. Nucl. Sci.* 89CH2669-0 : 1736-1740 (1989)
14. Stiening, R., *AIP Conf. Proc.* 105: p. 281 (1982)
15. Phinney, N., *IEEE Trans. Nucl. Sci.* 32: p. 2117 (1985)
16. Picasso, E., *Proc. EPAC 88 Conf.*, ed. Tarzzari, World Scientific Inc., Singapore: 3 (1988)
17. Bachy, G., et al. *Part. Accel.* 26: 19-31 (1990)
18. Richter, B., *Nucl. Instrum. & Methods*, 47, 136 (1976)
19. Abrams, G. S., et al. *Phys. Rev. Lett.* 63: 724-727 (1989)
20. Abrams, G. S., et al. *Phys. Rev. Lett.* 63: 2173-2176 (1989)
21. Kurokawa,S., Nakayama, H., Yoshioka,M., eds. *2nd Int. Workshop on Next-Generation Linear Collider*, KEK Report 90-22, Tsukuba, KEK: Japan (1990).
22. Tigner, M., *Nuovo Cimento* 37:1228-1231 (1965)

23. Amaldi, U., *Phys. Lett.* B61: 313-315 (1976)
24. Skrinsky, A., *Proc. 6th Natl. Accel. Conf.* Dubna, v.1: 19 (1978)
25. Sands, M., *SLAC-Report-121.* Stanford: SLAC (1970)
26. Abrams, G. S., et al., *Nucl. Instrum. Methods.* A 281: 55 (1989)
27. Breidenbach, M., et al., *SLAC-PUB-3798,* Stanford: SLAC (1985)
28. Breidenbach, M. et al., *SLAC-SLC-1991,* Stanford: SLAC (1990)
29. James, M. B., Miller, R. H., *IEEE Trans. Nucl. Sci.* 28: p. 3461 (1981)
30. Clendenin, J. E., et al., *IEEE Trans. Nucl. Sci.* 28: p. 2452 (1981)
31. Sheppard, J. C., et al., *IEEE Trans. Nucl. Sci.* 87CH2387-9: 43-46 (1987)
32. Herrmannsfeldt, W. B., *SLAC-TN-68-36.* Stanford: SLAC (1968)
33. Herrmannsfeldt, W. B., *SLAC-PUB-4623.* Stanford: SLAC (1988)
34. Ross, M. C., et al., *IEEE Trans. Nucl. Sci.* 32: p. 3160 (1985)
35. Bane, K. L. F., *SLAC-CN-16.* Stanford: SLAC (1980)
36. Bane, K. L. F., *AIP Conf. Proc.* 153: 971 (1985)
37. Steining, R., *SLAC-CN-40.* Stanford: SLAC (1981)
38. Clendenin, J. E., et al., In *Proc. 1988 Linear Accel. Conf.* CEBAF Report--89-001: p. 568 (1988)
39. Bulos, F., et al., *IEEE Trans. Nucl. Sci.* 32:1832-1834 (1985)
40. Clendenin, J. E., et al., *Part. Accel.* 30: 85-90 (1990)
41. Kulikov, A., et al., *SLAC-PUB-5473.* Stanford: SLAC (1991)
42. Ecklund, S. D., *AIP Conf. Proc.* 184: p. 1592 (1988)
43. Ecklund, S. D., *SLAC-CN-128* Stanford: SLAC (1981)
44. Reuter, E., et al., *SLAC-PUB-5370.* Stanford: SLAC (1991)
45. Reuter, E., et al., *SLAC-PUB-5369.* Stanford: SLAC (1991)
46. Kulikov, A., et al., *SLAC-PUB-5474.* Stanford: SLAC (1991)
47. Hutton, A., et al., *IEEE Trans. Nucl. Sci.* 32: p. 1659 (1985)
48. Rivkin, L. Z., et al., *IEEE Trans. Nucl. Sci.* 32: p. 1659 (1985)
49. Fischer, G. E., et al., *Proc. 12th Intl. Conf. on High Energy Accel.*, ed. F. T. Cole, R. Donaldson, Batavia, Ill.: p. 37 (1983)
50. Mattison, T. S., et al., *Part. Accel.* 30: 115-120 (1990)
51. Mattison, T. S., et al., *SLAC-PUB-5462.* Stanford: SLAC (1991)
52. Bane, K. L. F., *SLAC-PUB-5177.* Stanford: SLAC (1990)
53. Wiedemann, H., *SLAC-CN-57.* Stanford: SLAC (1981)
54. Fieguth, T. H., Murray, J. J., *Proc. 12th Intl. Conf. on High Energy Accel.*, ed. F. T. Cole, R. Donaldson, Batavia, Ill.: p. 401 (1983)
55. Brown, K., *SLAC-PUB-2257.* Stanford: SLAC (1979)
56. Corredoura, P. L., et al., *IEEE Trans. Nucl. Sci.* 89CH2669-0: 1879 (1989)
57. Seeman, J. T., Sheppard, J. C., *In Proc. 1986 Linear Accel. Conf.*, ed. G. Loew, SLAC-Report-303. Stanford: SLAC p. 214 (1986)
58. Balakin, V., et al., In *Proc. 12th Int. Conf. on High Energy Accel.*, ed. F. T. Cole, R. Donaldson, p.119. Batavia, Ill: Fermi Nat. Accel. Lab. (1983)
59. Allen, M. A., et al., *IEEE Trans. Nucl. Sci.* 87-CH2387-9: 1713-1715 (1987)
60. Farkas, Z. D., et al., *SLAC-PUB-1561.* Stanford: SLAC (1975)
61. Jobe, R. K., et al., *IEEE Trans. Nucl. Sci.* 87CH2387-9: 735-737 (1987)
62. Bane, K. L. F., *SLAC-AP-76* : Stanford: SLAC (1989)
63. Seeman, J. T., et al., In *Proc. 1986 Linear Accel. Conf.* Stanford: SLAC-Report-303, p. 441 (1986)
64. Seeman, J. T., et al., *SLAC-PUB-5438.* Stanford: SLAC (1991)
65. Abrams, G. S., et al., *Part. Accel.* 30: 91-96 (1990)
66. Hsu, I., et al., In *Proc. 1990 Linear Accel. Conf.*, Los Alamos Matl. Lab., LA-12004-C: p. 662 (1990)
67. Sheppard, J. C., *IEEE Trans. Nucl. Sci.* 32: 2180 (1985)
68. Seeman, J. T., *SLAC CN-251.* Stanford: SLAC (1983)

69. Herrmannsfeldt, W. B., et al. *Applied Optics* 7: 996 (1968)
70. Lavine, T. L., et al., *SLAC-PUB-4720*. Stanford: SLAC (1988)
71. Fischer, G. E., *SLAC-Report 358*. Stanford: SLAC (1990)
72. Fischer, G. E., et al., *IEEE Trans. Nucl. Sci.* NS-32-5: 3657-3659 (1985)
73. Weng, W. T., et al., *IEEE Trans Nucl. Sci. NS*-32-5: 3660-3662 (1985)
74. Weng, W. T., Sands, M., *SLAC-CN-339*. Stanford: SLAC (1986)
75. Barklow, T. L., et al., *Part. Accel.* 30: 121-126 (1990)
76. Bambade, P., Hutton, A., *SLAC-CN-370*. Stanford: SLAC (1989)
77. Pitthan, R., et al., *IEEE Trans. Nucl. Sci.* 87-CH2387-9: p. 1402 (1987)
78. Stiening, R., *SLAC-CN-20*. Stanford: SLAC (1980)
79. Sand, M., *SLAC-CN-326*. Stanford: SLAC (1986)
80. Kheifets, S. A., et al., *Part. Accel.* 30: 79-84 (1990)
81. Waltz, D., *Proc. 1st Intl. Workshop on Next Generation Linear Collider*. ed. M. Riordan, SLAC-Report-335, Stanford: SLAC p. 262 (1988)
82. Brown, K. L., *SLAC-PUB-4159*. Stanford: SLAC (1987)
83. Erickson, R. A., *AIP Conf. Proc.* 184: p. 1553 (1988)
84. Murray, J. J., et al., I*EEE Trans. Nucl. Sci.* 87-CH2387-9: p. 1331 (1987)
85. Hawkes, C. M., Bambade, P., *SLAC-PUB-4621*. Stanford: SLAC (1988)
86. Erickson, R. E., et al., *IEEE Trans. Nucl. Sci.* 87-CH2387-9: p.142 (1987)
87. Breidenbach, M., et al., *SLC Performance in 1991*, SLAC Report. Stanford: SLAC (1990)
88. Bambade, P., et al., *SLAC-PUB-4776* Stanford: SLAC (1989)
89. Hirata, K., et al., *Phys. Lett.* B224: 437 (1989)
90. Bambade, P., et al., *Phys. Rev. Lett.* 62: 2949 (1989)
91. Bonvicini, G., et al., *Phys. Rev. Lett.* 62: 2381 (1989)
92. Ziemann, V., *SLAC-PUB-5479*. Stanford: SLAC (1991)
93. Hollebeek, R., *AIP Conf. Proc.* 184: p. 680 (1988)
94. Jacobsen, R., et al., *SLAC-PUB-5205*. Stanford: SLAC (1990)
95. Levi, M., *SLAC-PUB-4922*. Stanford: SLAC (1989)
96. Ross, M. C., *IEEE Trans. Nucl. Sci.* 87-CH2387-9: p. 508 (1987)
97. Phinney, N., Shoaee, H. *IEEE Trans. Nucl. Sci.* 87-CH2387-9: P. 789 (1987)
98. Neal, R. B., *The Stanford Two-Mile Accelerator*, W. A. Benjamin, Inc., New York (1968)
99. Thompson, K. , Phinney, N., *IEEE Trans. Nucl. Sci.* 32: 2123-2125 (1985)
100. Ross, M. C., *SLC Experiment Note 202*. Stanford: SLAC (1990)
101. Pellegrin, J. L., et al, *IEEE Trans. Nucl. Sci.* 87-CH2387-9: p. 673 (1987)
102. Ross, M. C., et al., *IEEE Trans. Nucl. Sci.* 32: p. 2003 (1985)
103. Ross, M. C., *SLC Experiment Note 179*. Stanford: SLAC (1990)
104. Field, R. C., et al., *Nucl. Instrum. Methods* A274: 37 (1989)
105. Ross, M. C., et al., *IEEE Trans. Nucl. Sci.* 87CH2387-9: 725-728 (1987)
106. Jobe, R. K., et al., *IEEE Trans. Nucl. Sci.* 87CH2387-9: 713-715 (1987)
107. Himel, T. H., *SLC Experiment Report 210*. Stanford: SLAC (1991)
108. Seeman, J. T., *IEEE Trans. Nucl. Sci.* 89-CH2669-0: p. 1736 (1989)
109. Emma, P., et al., *SLAC-CN-381*. Stanford: SLAC (1991)
110. Spence, W. L., et al., *SLAC-PUB-5276*. Stanford: SLAC (1990)
111. Sheppard, J. C., *SLAC-CN-298*. Stanford: SLAC (1985)
112. Seeman, J. T., *SLAC-CN-330*. Stanford: SLAC (1986)
113. Merminga, N., et al., *SLC Experiment Report 172*. Stanford: SLAC (1991)
114. Servranckx, R., Brown, K., *SLAC-CN-350*. Stanford: SLAC (1986)
115. Bane, K. L. F., Wilson, P., *Proc. 11th Intl Conf. High Energy Accel.*, Geneva, Birkhauser Verlag: p. 592 (1980)
116. Seeman, J. T., Sheppard, J. C., *Proc. of Workshop on New Developments on Part. Accel. Techniques*, ed. Turner, Orsay: CERN-87-11, p. 122 (1987)

117. Seeman, J. T., *SLAC-PUB-4968*. Stanford: SLAC (1991)
118. Seeman, J. T., Merminga, N., In *Proc. 1990 Linear Accel. Conf.*, Los Alamos Natl. Lab., LA-12004-C: p. 387 (1990)
119. Balakin, V., *Proc. of 1st Intl. Workshop on Next-Generation Linear Collider*. Stanford: SLAC-Report-335, P. 56 (1988)
120. Seeman, J. T., *SLC Experiment Report 221*. Stanford: SLAC (1991)
121. Adolphsen, C. E., et al., *SLAC-PUB-4902*. Stanford: SLAC (1989)
122. Raubenheimer, T., Ruth, R. D., *SLAC-PUB-5355*. Stanford: SLAC (1991)
123. Seeman, J. T., In *Proc. 1990 Linear Accel. Conf.*, Los Alamos Natl. Lab., LA-12004-C: p. 390 (1990)
124. Chao, A., et al., *Nucl. Instrum. Methods* 178:1 (1980)
125. Stiening, R., *SLAC-CN-161*. Stanford: SLAC (1982)
126. Seeman, J. T., et al., *SLAC-PUB-5437*. Stanford: SLAC (1991)
127. Seeman, J. T., et al., *IEEE Trans. Nucl. Sci.* 32: p. 2629 (1985)
128. Stiening, R., *SLAC-CN-181*. Stanford: SLAC (1982)
129. Seeman, J. T., *IEEE Trans. Nucl. Sci.* 87-CH2387-9: p. 1267 (1987)
130. Seeman, J. T., *Part. Accel.* 30: 73-78 (1990)
131. Stiening, R., *SLAC-CN-42*. Stanford: SLAC (1981)
132. Fischer, G. E., *AIP Conf. Proc.* 153: p. 1047 (1984)
133. Bane, K. L. F., Morton, P., *Proc. 1986 Linear Accelerator Conf.*, ed. G. Loew, Stanford: SLAC p. 490 (1986) and SLAC-Report-303: 490 (1986)
134. Merminga, N., et al., *SLAC-PUB-5436*. Stanford: SLAC (1991)
135. Toge, N., et al. *IEEE Trans. Nucl. Sci.* 89-CH2669-0: p. 1844 (1989)
136. Seeman, J. T., et al., *Part. Accel.* 30: 91-96 (1990)
137. Clendenin, J. E., et al., *SLAC -PUB-5368*. Stanford: SLAC (1991)
138. Moffeit, K. C., *Proc. Minneapolis Spin Conf.* , S. Smith ed., U. Minnesota, Minneapolis, p. 901 (1988)
139. Clendenin, J. E., *SLAC-PUB-5368*. Stanford: SLAC (1990)
140. Chao, A., *SLAC-CN-29*. Stanford: SLAC (1980)
141. Panofsky, W. K. H., *SLAC CN-383*. Stanford: SLAC (1991)
142. Maruyama, T., et al., *SLAC-PUB-5420*. Stanford: SLAC (1990)
143. Seeman, J. T., *SLAC CN-377*. Stanford: SLAC (1991)